arXiv:2505.02826v1 [cond-mat.stat-mech] 5 May 2025

Statistical mechanical theory of liquid water

Lakshmanji Verma *[1] and Ken Dill †[1,2]

[1] *Laufer Center for Physical and Quantitative Biology, Stony Brook University, NY, USA*
[2] *Department of Physics & Department of Chemistry, Stony Brook University, NY, USA*

May 6, 2025

Abstract

Water is an unusual liquid. Its thermophysical properties are non-monotonic with temperature T and pressure p. It's not been known how water's behaviors are encoded in its molecules. We give a statistical physics model, *Cage Water*, which assumes three bonding states: van der Waals, pairwise hydrogen bonding, and multi-body cooperative caging hydrogen bonds. The model is analytical, so very fast to compute, yet it gives excellent agreement with extensive pT experiments. Through readily interpretable substates, Cage Water explains water's liquid anomalies – including its controversial liquid-liquid supercooling transition – as simple switchovers among the three bonding types.

Introduction

Water is one of the most computer-simulated molecules in the world, because of its major roles in biology, chemistry, physics and geoscience. Yet, it remains poorly understood. Liquid water is unusual in having a density maximum in its liquid temperature range, a change in sign of its thermal expansion, minima in both its compressibility and heat capacity, and an apparent liquid-liquid critical point in its supercooled region. We seek explanations that are rooted in the structure and energetics of individual water molecules. There have been two general approaches to physical modeling of water's structure property relationships.

First, water has been simulated by computations of ever-improving atomistically detailed models, such as ST2, TIP, SPC, OPC, rWAIL, and mW [1, 2, 3, 4, 5, 6, 7, 8, 9], or polarizable models such as MB-pol, TTM, iAMOEBA, and MB-UCB [10, 11, 12, 13, 14, 15], or machine learning (ML) and neural network (NN) models trained on *ab initio* data

*Contributing author: lakshmanji.verma@stonybrook.edu
†Corresponding author: dill@laufercenter.org

[16, 17, 18, 19, 20, 21, 22, 23, 24, 25]. These approaches offer the most uncorrupted grounding in atomistic physics; typically quite good agreement with experimental data; and good transferability across different application venues. But computer simulations have limitations: (i) They are *computationally expensive.* As modeling challenges become ever bigger, especially in biology, today's water modeling doesn't scale well. (ii) Simulations produce *trajectories,* which are fluctuating vectors that become interpretable only upon converged averaging over multiple runs. They have sampling errors, so computed heat capacities and other derivatives of free energies are challenging. For these reasons, a major controversy took years – and multiple forcefields – to resolve; namely the nature of the supercooled liquid transition [26, 27, 28, 29, 30]. (iii) Simulations lack *interpretability.* They are snapshots, not explanations. MD trajectories are strings of stochastic many-atom, many-bond, many-configuration microstates. While such modeling often reproduces water's properties, it doesn't explain them.

A second approach is more coarse-grained, based on defining mesostates – such as hydrogen bonded, or in ice-like clusters, or having different local water densities, for example. This approach arguably began with Roentgen in 1892 [31], who interpreted liquid water as having two components of different densities. Bernal and Fowler [32] identified the importance of hydrogen bonding in ice structure and Pauling [33] estimated the residual entropy of ice from hydrogen arrangements between the oxygen. Pople [34] suggested the existence of a continuum of distorted hydrogen bonds. In contrast, Davis and Litovitz [35] and Angell [36] proposed two-state models, consisting of ice-like open hexagonal waters and closed-packed waters. Other two-state thermodynamic theories [37, 38, 39, 40, 41] posit that water anomalies are a result of competition between a less ordered high-density liquid (HDL) and a more ordered low-density liquid (LDL) water states, reviewed in detail by Gallo *et al.* [42]. In recent advances, the otherwise incommensurate tetrahedral and spherical symmetries can now be treated together within a single framework [43, 44, 45]. In the Franzese-Stanley model (FS) [44, 45], water molecules are placed onto lattice sites and interact with neighboring waters through mean-field Ising contact and orientational interactions, in addition to a 3-body cooperative tetrahedrality energy term [46]. But the FS model relies on simulating Monte Carlo trajectories. Here, we aim for a more analytical theory instead.

We build upon a model of Urbic [43], which is off-lattice, reckons with pairwise Lennard-Jones and pairwise hydrogen bond interactions and has a 12-body ice-like cooperativity energy. But here we introduce translational and volumetric physics, replacing prior simplifications. The present model, *Cage Water*, starts from a partition function, so it is analytical, not sampled; thus orders of magnitude faster than a simulation. The novelty of this model is in bridging from interpretable molecular physics on the one hand, to making excellent predictions of extensive thermophysical experiments on the other hand. It also gives insights into a controversy about water's supercooled liquid-liquid transition.

Theory of the Three Bond Types

We define four different mesostates of liquid water, figure 1, similar to the Cage Water model [47]: i) isolated non-interacting water molecules, such as those in the vapor phase (NI); ii) water pairs that do not have a hydrogen bond but interact through a van der Waals (vdW) type interaction; (iii) water pairs that interact through a hydrogen bond (pHB); and iv) a fully hydrogen-bonded cooperative ice-like cage (cage) in the liquid state. Below, we define the statistical mechanical weights of these four states, cum them into a partition function, and solve for the various state populations as functions of temperature and pressure.

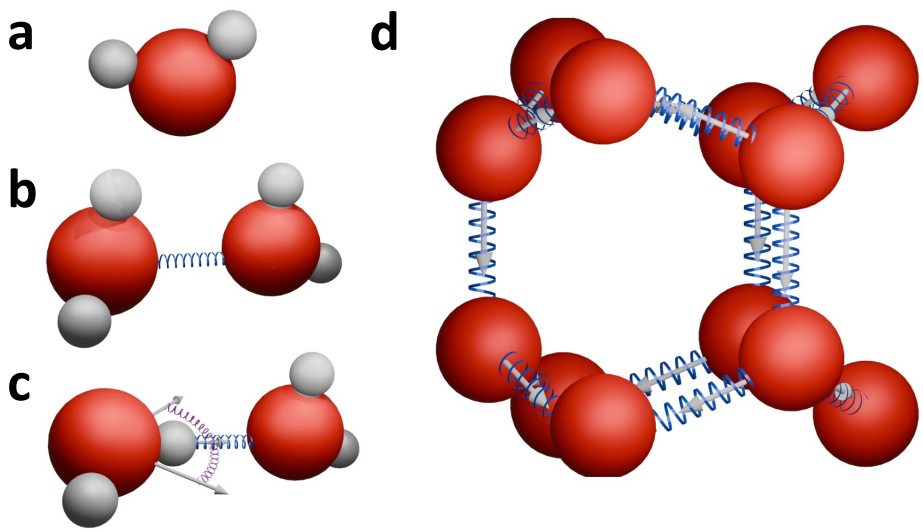

Figure 1: **Cage Water's four microstates. a)** Non-interacting (NI) monomer water. b) Pair van der Waals (vdW) interaction. Translational spring in blue. **c)** Pair HB (pHB) state with HB arms shown with an arrow. Orientational springs (purple) and the HB arms (arrows) indicate dynamic HBs. **d)** A 12-member cooperative cage (cage) unit of Ih ice, showing connecting translational springs. a,b,c) Oxygen atoms are shown with red balls and hydrogen atoms are shown with silver balls. Hydrogen atoms are not shown in **d)** for clarity

First, we estimate the volumes of four states from a reference water species, Ih ice. We model the liquid water cage state in the limit of the Ih ice cage, consisting of 12-membered building units of water cages. We geometrically estimated the equilibrium volume of the cage per water molecule,

$$v_{cage} = \frac{8\sqrt{3}\sigma_{Ih}^3}{9} = A_{cage}\sigma_{Ih}^3, \tag{1}$$

where σ_{Ih} is the water-water distance in the Ih ice cage. We perturb the cage water to model pHB state, $A_{pHB} = x_{pHB} \times A_{cage}$, and vdW state, $A_{vdW} = x_{vdW} \times A_{cage}$, and NI state in in the vapor limit, $v_{NI} = v_{vdW} + T/p$. We allow σ_j of each state to contract or expand in response to the thermodynamic condition to capture the translational contributions. See the

supplementary information (SI) for details.

We model the direction HB interaction, equation 2, with an attractive constant part $-\epsilon^0_{pHB}$, a restoring orientation-dependent harmonic potential with spring constant κ_Θ with equilibrium angle between arms $\Theta = 0$ where the rotational penalty is 0.

$$\epsilon_{pHB} = -\epsilon^0_{pHB} + \kappa_\Theta(1 - \cos(\Theta))^2 \; ; \qquad for - \pi/6 <= \Theta <= \pi/6. \tag{2}$$

Interactions in cooperative cages differ from the HB interaction by an additional attractive term, $\epsilon_{cage} = \epsilon_{pHB} - \epsilon_c$. Whereas vdW state only consists of the constant attractive term,

$$\epsilon_{vdW} = -\epsilon^0_{vdW}. \tag{3}$$

We capture the translational contribution to energy due to the contraction and expansion of volumes with a restoring harmonic potential, $\kappa_x \langle \Delta x \rangle^2$ with a spring constant κ_x and with the same translational limits as volumes, see SI for details.

Following experimental observations and for simplicity, we assume that each water in the three states, cage, pHB, and vdW, interacts with four neighboring water molecules. There would be an additional $6k_BT$ to the overall energy per water molecule, which accounts for equally partitioned bond vibration energy for four bonds. We can estimate the effective interaction energy per water molecule as,

$$u_j = -2\epsilon_j + \kappa_x \langle \Delta x \rangle^2 + 6k_BT \tag{4}$$

Interaction energy for NI state is zero i.e. $u_{NI} = 0$.

Now we estimate the Boltzmann weights for states, $\Delta_{cage}, \Delta_{pHB}, \Delta_{vdW}$, and Δ_{NI}, with energy u_j and volume v_j, in an isothermal-isobaric (NpT) ensemble by integrating over rotational degrees of freedom Φ, Ψ, and Θ and translational degrees of freedom x, y, and z, see the SI for details.

From these Boltzmann weights, we estimate the partition function for the 12-membered single cage as

$$Q_1 = (\Delta_{pHB} + \Delta_{vdW} + \Delta_{NI})^{12} - \Delta^{12}_{pHB} + \Delta^{12}_{cage}. \tag{5}$$

Here, the first term accounts for many-body combinations, up to 12th order, of the three water states, HB, vdW, and NI, contributing to 12 water molecules. We assume there is additional cooperative energy when all 12 waters in the cage are hydrogen bonded with each other. To capture this cooperativity, we replace the 12th order pair HB contribution Δ^{12}_{pHB}, the 2nd term with Δ^{12}_{cage}, the 3rd term. The partition function for one water effectively would be given by $q_b = Q_1^{1/12}$.

We model the attraction between 12-membered cages with a self-consistent mean-field approximation similar to Truskett and Dill (TD) [48]. The additional dispersion interaction

between N molecules is $-Na/\langle v_{mol}\rangle$, where a is the van der Waals dispersion term between cages and $\langle v_{mol}\rangle$ is the molar volume of single water molecules. This dispersion term reduces the system's pressure from p_0 to $p = p_0 - a/\langle v_{mol}\rangle^2$. So, to estimate properties at pressure p, we evaluate them at higher pressure p_0 such that

$$p_0 = p + a/\langle v_{mol}\rangle^2. \tag{6}$$

We then obtain water's thermophysical properties using standard thermodynamic relationships [49] from the partition function [48, 47, 50, 43].

How the model explains liquid water's properties

A purpose of this model is to provide a microscopic interpretation of water's liquid across temperature and pressure, based on the calculated populations (f_{cage}, f_{pHB}, & f_{vdW}) of the microstates, figure 2b. Here we compare the model predictions: (i) to experiments and (ii) to the TIP4P/2005 [3, 51] and to MB-pol [10] explicit water models, which are often regarded as the state-of-the-art atomistic models for pure liquid water at least at ambient pressure.

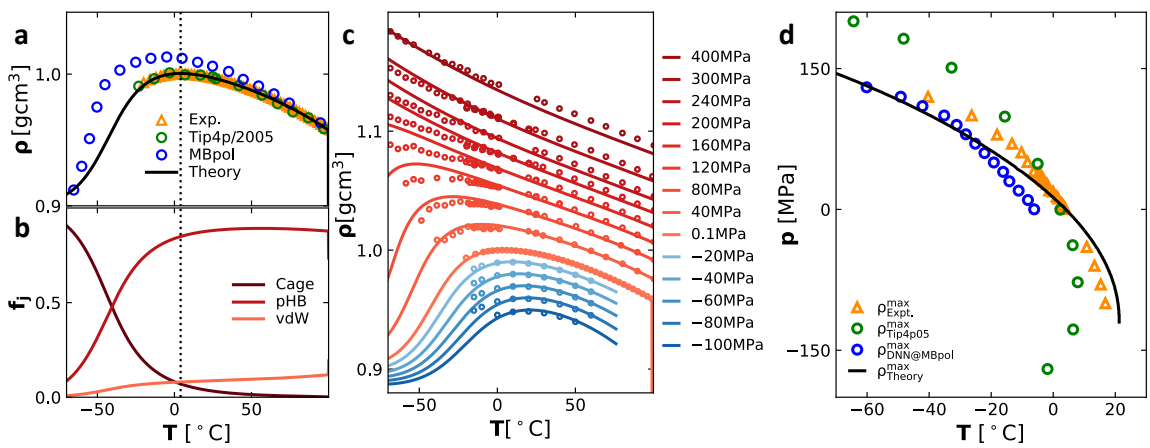

Figure 2: **Liquid water's density vs. temperature and pressure, predictions and experiments. a)** Density vs. temperature at atmospheric pressure: model (solid black line); experiments[52, 53] (orange open triangles); TIP4P (open green circles); MB-pol (open blue circles). **b)** The computed populations of the three model microstates. The dotted line in **a, b** indicates the temperature of maximum density, 4 °C. **c)** Density isobars for non-ambient pressures. Theory predictions for $p > 0$ are shown in red and for $p < 0$ in blue. Circles are the experimental data points. **d)** Maximum density prediction in comparison with experiments (orange triangles), TIP4P (green circles), and DNN@MBpol [54] (blue circles). Pressures are in MPa.

Water's density, a balance of open and compact structures

We compute water's density from the molar volume, v_{mol}, with typical density relation $\rho = M_w/v_{mol}N_A$, where $M_w = 18\ g/mol$ is molecular weight of water per mole and $N_A =$

6.022×10^{23} $molecules/mol$ is the Avogadro number. Figure 2 shows that this model quantitatively predicts the density for the entire range pT (-100 MPa to 400 MPa & $-75°C$ to $150°C$) explored experimentally [52, 53]. At atmospheric pressure, the prediction is as accurate as that of TIP4P/2005 and MB-pol. It predicts a density maximum around 4°C, shown with a vertical dotted line in figure 2a, and also the boiling at 100°C (see figure **??**).

At temperatures colder than ≈ -45°C, where cage and pHB states crossover, the cage state dominates owing to its stronger cooperative energy, resulting in highly ordered ice-like low-density cagey water. At warmer temperatures, pHB water dominates, due to its smaller volume than cage water and stronger interactions than vdW water, causing density to increase until a crossover between vdW and cage state near 4°C. Beyond this point, vdW water population increases significantly due to its higher translational and rotational entropy, causing the density to decrease, resulting in a maximum at 4°C.

Figure 2c shows predicted density-temperature curves for different pressures. First, as expected, water's density increases with pressure. Figure S2 shows the model prediction that increasing pressure crunches cages into pHB pieces. Figure S3 shows that the two crossover points, from f_{cage} to f_{pHB} and from f_{cage} to f_{vdW}, shift to lower temperatures with increased pressure, resulting in the temperature of maximum density (TMD) shifting towards a lower temperature with pressure. Figure 2d experimental predictions that are comparable to, or better than, those of TIP4P/2005 and the deep neural network surrogate of MB-pol (DNN@MB-pol) [54]. Under stretchable pressures, $p < 0$, TMD undergoes a turnaround point, resulting from the nonmonotonic behavior of f_{vdW}. It increases with pressure in cold water, $T <\approx 10$°C until it plateaus at $\approx 9\%$, figure S2c.

Two-state models [36, 37, 38, 39, 40, 41, 42, 55] treat the water anomalies as a competition between a less ordered high-density liquid (HDL), and a highly ordered low-density liquid (LDL). These models capture supercooled water properties quite well. However, the presence of highly ordered LDL at warmer temperatures is counterintuitive. Ricci et al. [56] found experimentally that this highly ordered LDL water predominantly exists at much colder temperatures. This suggests a presence of different low-density water that is less ordered, the vdW water in this model, and its population increases due to the breaking of more HBs at warmer temperatures, causing the density to decrease. This is also supported by the findings of Morawietz et al. [16] where van der Waals interactions were crucial to reproducing density maximum in an *ab initio* quality NN water potential. Under moderate stretchable pressure, $p < 0$, more HB water are broken into vdW water due to tension. This increase in weak vdW population stabilizes water as it allows water to expand and thus nullifies the tension, figure S2c.

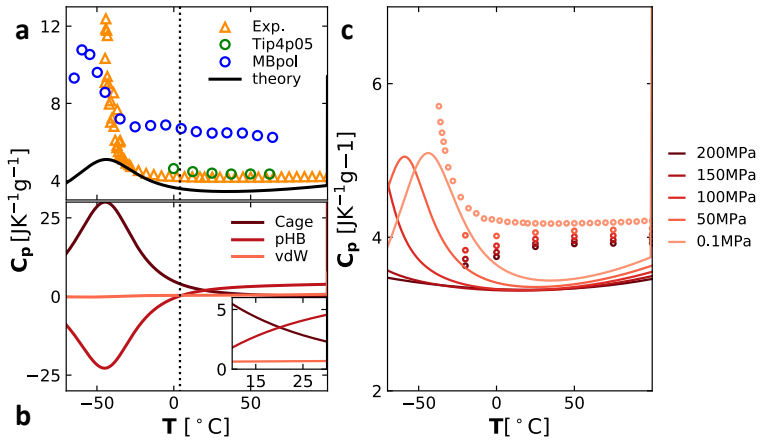

Figure 3: **Heat capacity, C_p, and its components vs temperature. a)** C_p at atmospheric pressure. **b)** Model component contributions to C_p. **c)** C_p isobars. Pressures are in MPa. Legends are the same as in figure 2. Experimental data is taken from ref. [57, 58, 59, 60].

Heat capacity minimum bonding transition: cage HB → pHB

We calculate the heat capacity from the enthalpy using the thermodynamic relationship

$$C_p = \frac{\partial \langle h \rangle}{\partial T} = \sum_j \frac{\partial (f_j \langle h_j \rangle)}{\partial T} \equiv \sum_j C_{p,j}, \tag{7}$$

here $C_{p,j}$ is the contribution from the jth state. Figure 3 shows agreement with experiments no worse than TIP4P/2005 or MB-pol at ambient temperatures. It also captures the anomalous increase in the supercooled region. The pronounced minimum (compared to a subtle minimum observed in experiments [61]) is around 35°C, which results from the dominant contribution switch from cage to pHB, see figure 3b. The maximum deviation from the experiment is near this minimum, $\approx 0.6\ J/gK$, which is reasonable. At lower temperatures, the contribution from breaking of cages dominates which causes C_p to increase until it peaks, C_p^{max}, around −44°C, figures 3b. Confined water experiments [62, 58, 63] as well as theories (MD simulations [64, 51], equation of state models [64, 41, 65], and recent statmech based model [46]) exhibit such peaks. At high pressure, figure 3c shows that predicted C_p, similar to experiment, decreases with pressure at ambient temperature and C_p^{max} shifts to a lower temperature (see figure S4) similar to TMD. This is a consequence of the shift in the crossover point between the cage and pHB water to a lower temperature with pressure, figure S3.

Compressibility minimum bonding transition: cage HB → vdW

We calculate the isothermal compressibility as the volumetric fluctuations in the molar volumes, $\langle v_{mol} \rangle$ with respect to pressure as,

$$\kappa_T = -\frac{\partial \ln \langle v_{mol} \rangle}{\partial p} = -\frac{1}{\langle v_{mol} \rangle} \sum_j \frac{\partial f_j \langle v_j \rangle}{\partial p} \equiv \sum_j \kappa_{T,j}, \tag{8}$$

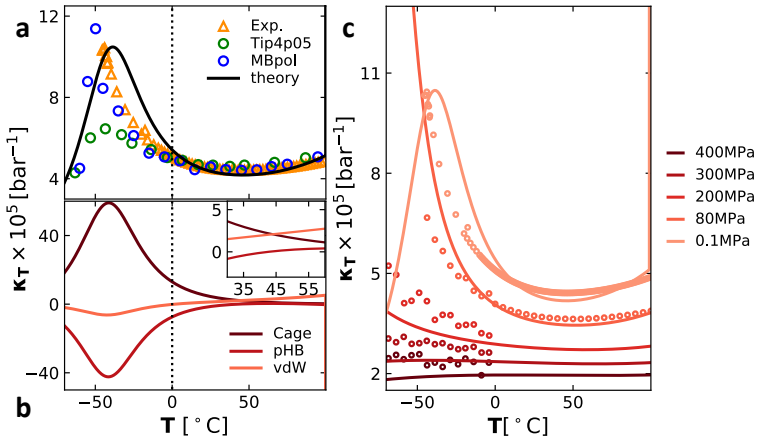

Figure 4: **Isothermal compressibility, κ_T, and its components vs temperature. a)** κ_T at atmospheric pressure. **b)** Microscopic components of κ_T. The inset zooms in at the cage $\rightarrow$ vdW crossover. **c)** κ_T isobars. Pressures are in MPa. Legends are the same as in figure 2. Experimental data is taken from ref. [52, 66, 67].

where $\kappa_{T,j}$ is the compressibility of state type j. Figure 4 shows that the model predictions are as good as TIP4P/2005 and at 1 atm at ambient conditions and captures much broader experimental data. The anomalous minimum, κ_T^{min}, near ≈ 45°C is understood through the model as a switchover the dominance of cages to vdW waters; see the inset of figure 4b. Below this temperature, the increase in κ_T is due to an increase in the dominant contribution from cage waters, more compressible than pHB waters, which also peaks near the κ_T^{max} at ≈ -40 °C in figure 4a, in excellent agreement with the observed value, κ_T^{max} at ≈ -44 °C [67]. In addition, sound velocities [68] and confined-water experiments [69] as well as computational and theoretical studies [70, 41, 71, 10] also report κ_T^{max} in supercooled water. Figure 4c shows that κ_T decreases with pressure, and κ_T^{max} shifts to a lower temperature with pressure (see figure S4).

Thermal expansion bonding transition: pHB $\rightarrow$ vdW

We calculate the expansion coefficient as the volumetric fluctuations in the molar volumes, $\langle v_{mol} \rangle$ with respect to temperature,

$$\alpha_p = \frac{\partial \ln \langle v_{mol} \rangle}{\partial T} = \frac{1}{\langle v_{mol} \rangle} \sum_j \frac{\partial f_j \langle v_j \rangle}{\partial T} \equiv \sum_j \alpha_{P,j}, \tag{9}$$

where $\alpha_{p,j}$ is the expansion coefficient of the jth state. Figure 5 shows that the current model captures the experimentally observed expansion coefficient for a broad pT range. The abnormal negative α_p below 4°C is the result of the dominant negative contribution from cage water, figure 5b. This reflects the loss of water's expandability as the more expandable pHB waters transition into less expandable cage waters with stronger and rigid HBs.

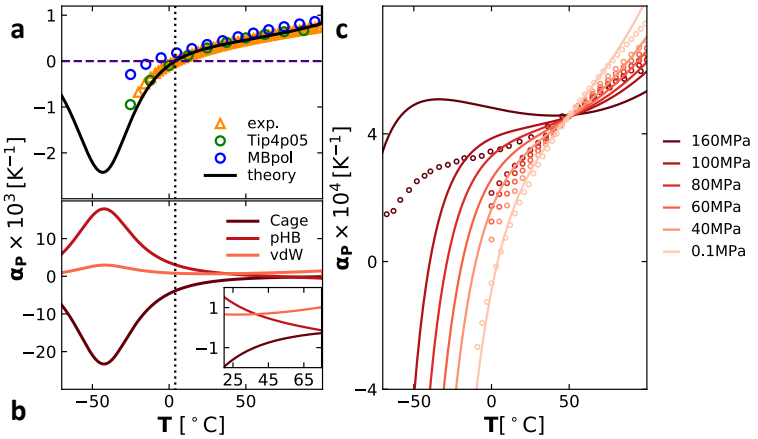

Figure 5: **Thermal expansion coefficient, α_p, and its components vs temperature. a)** α_p at atmospheric pressure. **b)** Microscopic components of α_p. The inset zooms in at the pHB $\rightarrow$ vdW and pHB $\rightarrow$ cage crossovers. **c)** α_p isobars. Legends are the same as in figure 2. Experimental data is taken from ref. [58, 66].

Similar to C_p^{max} and κ_T^{max}, α_p exhibits a minimum, α_p^{min}, in the supercooled region (see figure S4). However, in the normal temperature range, α_p isobars are nonmonotonic and crossover at $\approx$ 50°C, an inflection point where water stops behaving abnormally [58]. This model predicts a inflection near $\approx$ 48°C. Figures 5b and S3b shows a transition from pHB to vdW in the vicinity of the inflection point, suggesting more vdW liquid like expansion behavior beyond this crossover. Additionally, figure S2c shows that the change in f_{vdW} behavior beyond this inflection point is the cause behind the α_p isobars crossover around $\approx$ 50°C.

Supercooling liquid transition bonding transition: cage HB $\rightarrow$ pHB.

There has been controversy about supercooled water. Is there a liquid-liquid phase transition? Support for such a transition is shown in Figure 6, indicating a tendency towards an extremum in the heat capacity, compressibility, and expansivity upon lowering the temperature to around -44 °C [67, 60]. Such extrema are well-established indicators of a phase change. In 1992, Poole et al. [26] proposed that such peaks in C_p and κ_T indicate the existence of Liquid–Liquid Transition (LLT) line between a high density liquid (HDL) of some kind and low density liquid (LDL); it meets the locus of maximum correlation length in the single phase, the Widom Line (WL), at the Liquid–Liquid Critical Point (LLCP), known as the LLCP scenario. Subsequently, evidence has been sought in molecular simulations. Several atomistic simulations using ST2 models [26, 74, 75, 76] and TIP models [77, 78, 79, 70, 80] indicated the LLCP in the so-called *no man's land,* where water readily crystallizes into ice. In contrast, the mW model doesn't show an LLCP [5]. Limmer and Chandler argued that these MD simulations suffer from inadequate sampling and dependencies on forcefields, and that the transition being observed in the simulations was simply water's crystallization, But subsequently, Palmer et al. [29] showed the existence of two metastable liquid phases, LDL and HDL, in equilibrium with a crystalline state for the ST2 model at 228.6 K and 240 MPa,

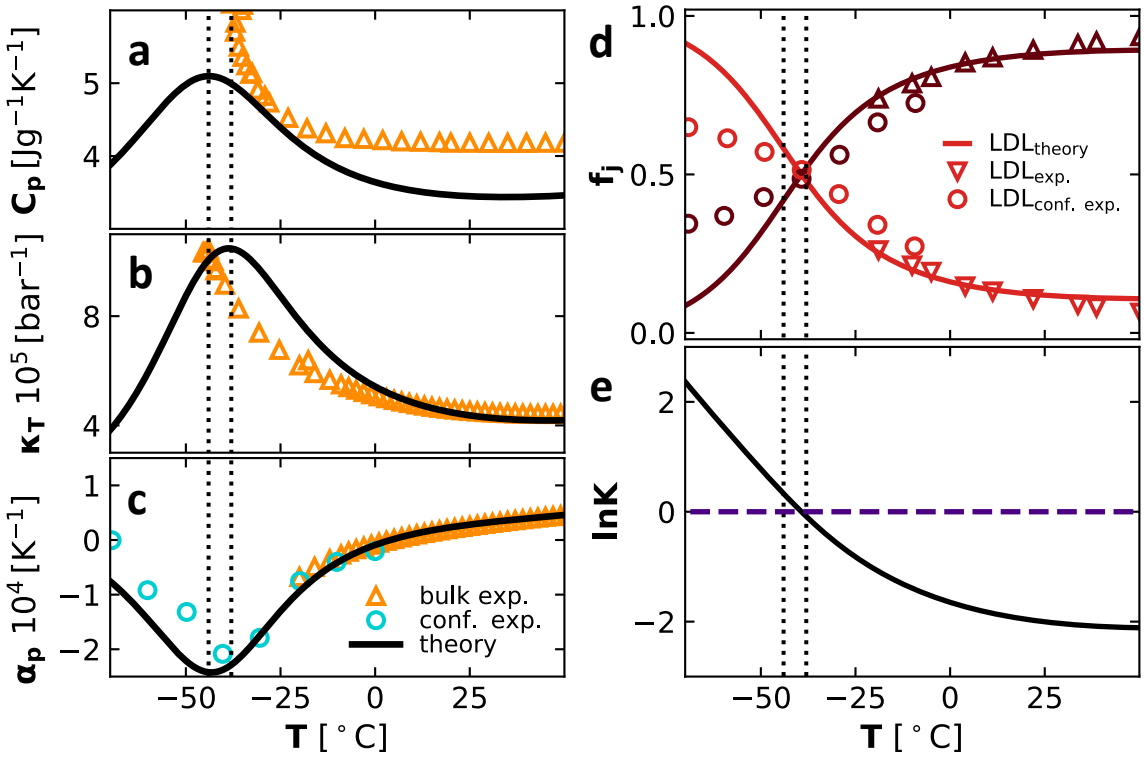

Figure 6: **Extrema in supercooled water at 1 atm are near HDL $\rightleftharpoons$ LDL equilibrium. a)** C_p, partial experimental data is shown to emphasize the predicted peak. **b)** κ_T. and **c)** α_p. **a)-c)** The model predictions (black solid lines), bulk water experiments [57](orange triangles), and confined water experiments [58](cyan triangles). **d)** Population of HDL (f_{HDL}) in brown and LDL (f_{LDL}) in red. Theory predictions are shown with solid lines, bulk experimental estimates of f_{LDL} taken from [72] and $f_{HDL} = 1 - f_{LDL}$ shown with open triangles, and confined experimental estimates are taken from [73] shown with open circles. **e)** $\ln K$ with vs temperature. $K = f_{LDL}/f_{HDL}$ is the equilibrium constant for the two-state system, HDL $\rightleftharpoons$ LDL.

independent of different advanced sampling methods.

More recent modeling and thermodynamic analyses have indicated the presence of LLT and LLCP points for supercooled water [71, 30, 81, 82, 9, 54, 83, 84, 55, 85]. Direct experimental observation of the LLT and LLCP have been elusive until recently. New experiments in ultrafast X-ray spectroscopic techniques have recently accessed the *no man's land* region of water's supercooled phase diagram [86, 67, 87, 60, 88, 89]. Kim et al. [87] provided direct experimental evidence of structural changes between HDL and LDL phases at 205 $\pm$ 10 K and pressure between 0.1 - 350 MPa on isochoric heating of high density amorphous ice (HDA), indicating an LLT. A similar experiment showed structural changes between HDL and LDL phases at 200 K on isochoric heating of low density amorphous ice (LDA) [89], further supporting the existence of LLT and LLCP scenario. However, the big range of estimates of pressure (from ambient to 350 MPa [87, 89]) imply that direct observation of

LLCP through experiments is still out of reach.

How does our Cage Water modeling add to this story? First, the challenge faced by all the MD studies is that they are simulations, requiring converged averages over trajectories that require extensive sampling of small free energy differences at very cold temperatures, where simulations are notoriously difficult [65, 29, 90, 70, 91, 92, 93, 69, 71, 94, 30, 54]. To converge on a story has required tests in multiple forcefields, and multiple long simulations. In contrast, the present model is analytical, with no concern about trajectories, sampling, small barriers or cold temperatures. The model is validated by good agreement with extensive liquid temperature and pressure experiments. Most importantly, the present model reveals a story that is expressed in meaningful subpopulations of water's forms of bonding. Some of the main players in the story – particularly the caging clusters – "punch above their weight", having importance for liquid state properties that is outsized compared to their very small populations. Details are below.

First, figure 6 a–c shows that the Cage Water model predicts the same telltale divergence features as experiments show of the supercooling anomaly, which occurs between -44 to -38 °C at atmospheric pressure. Second, while no bulk experiments have yet been able to reach temperatures low enough to probe the supercooling peak, experiments on nano-confined liquids can do so [73]; see the blue circles in Figure 6 c. The Cage Water model predicts that the supercooling peak point is precisely where the liquid undergoes a transition from a low-density liquid at lower temperatures to a high-density liquid at higher temperatures. Figure 6 e shows the experimentally observed crossover point [72]. And Figures 6 d and e show this experimental transition point to be where the model has a crossover from a dominant population of LDL (cage plus vdW) to a dominant population of HDL (pHB states).

Figure 7 shows that Cage Water captures well the thermophysics of water's supercooling. First, some basic expectations: The Liquid-Liquid Critical Point (LLCP) should be the point on the PT phase diagram where the Liquid-Liquid Phase Transition (LLPT) ends and the Widom Line (WL) begins (the loci of the maximum correlation lengths) and also where the response functions have their extrema ($C_p^{max}, \kappa_T^{max}$, and α_p^{min}) [45, 97]. If a system is two-state (in our case the high- and low-density phases, HDL $\rightleftharpoons$ LDL), then the LLCP point, the LLPT line, and the WL line should all be where $\ln K = 0$, where K is the equilibrium point of the transition [98]. Figure 7 shows this holds true for Cage Water. The model predicts the LLCP to be at 159 K and 176 MPa, figure 7a. Figure 7b shows the predicted transition curves, the critical point, the binodal curve, and the first-order nature of the transition below the critical temperature. As far as we know, there are no experimental measurements of the critical point yet. But our predicted critical pressure is within the expected range of $143-360$ MPa [26, 99, 74, 75, 76, 77, 78, 79, 70, 80, 29, 30, 100]. And ρ^{max} is in excellent agreement with the experiments. However, the model critical temperature is somewhat colder than the previously predicted range of $172-250$ K.

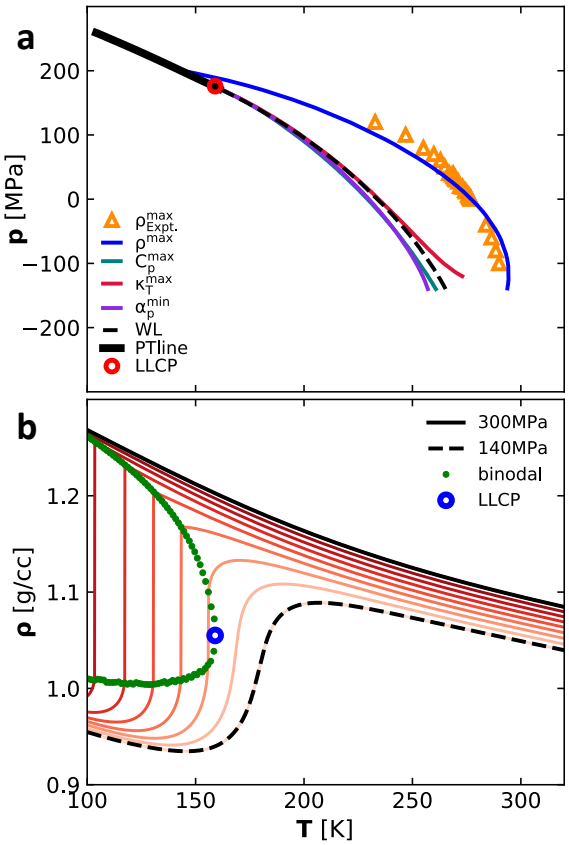

Figure 7: **The model captures the pressure dependence of the supercooling peak temperatures. a)** Model predictions of response function extrema are shown with solid lines; ρ^{max} in blue solid line, C_p^{max} in teal, κ_T^{max} in crimson, and α_p^{min} in violet. The predicted Widom line (WL) and phase transition (PT) line are shown with a black dashed line and a thick solid line, respectively. Experiments [53, 52, 95, 96] are shown with open orange triangles. **b)** Density isobars for a range of 140-300 MPa on an interval of 20 MPa, showing first-order phase transitions, are shown in shades of red. The phase boundary, the binodal line, is shown with green dots. The predicted liquid-liquid critical point at pressure 176 MPa and temperature 159 K is shown with an open red circle in panel **a)** and an open blue circle in panel **b)**.

The model energies are consistent with known values

The predicted water-water bond (dissociation) energy, $\langle u \rangle = \sum f_j u_j$, is temperature dependent but at room temperature, the model value is $\approx -12.7\ kJ/mol$(see figure S5). This is fairly consistent with different experiments: older thermal conductivity and infrared absorption data gives is $\approx -18 \pm 3kJ/mol$ [101, 102, 103, 104, 105, 106], while more recent estimates at room temperature using pressure broadening give $-13.6 \pm 4kJ/mol$ [107] and $-15.5 \pm 5.6\ kJ/mol$ [108], and velocity map imaging gives the $(H_2O)_2$ dissociation energy as $-13.2 \pm 0.12\ kJ/mol$ [109]. Within similarly large ranges, these values are consistent with the corresponding *ab initio* dissociation energy estimates of $D_0 \approx -13.2\ kJ/mol$ for $(H_2O)_2$ [110]. Experiments, however, don't give the microscopic components (vdW, pair HB, and

cooperative). The values of these quantities in the model are: maximum strength (in the absence of thermal contributions) of a vdW energy is $\epsilon \approx -10.3\ kJ/mol$, and pHB and cage water at the minimum energy configuration of HB, when the HB arms are aligned are $\epsilon^0_{pHB} \approx -19.2\ kJ/mol$ and $\epsilon^0_{cage} \approx -20.5\ kJ/mol$), respectively (figure S5b) which are also consistent with corresponding *ab initio* electronic dissociation energy $D_e \approx 21\ kJ/mol$ [110].

Conclusions

We describe here Cage Water, a statistical mechanical model of liquid water. It treats water's orientational and translational freedom and explains the liquid thermophysical properties and anomalies in terms of three interaction types: water-water vdW bonds of strength $\approx -10.3\ kJ/mol$, water-water Hbonds of strength $\approx -19.2\ kJ/mol$, and multi-water cage-structure Hbonds of strength $\approx -20.5\ kJ/mol$. In comparison with extensive temperature and pressure experiments, the Cage Water model is as accurate as explicit models TIP4P/2005 and MB-pol (for the pure liquid), but it has the advantages that it is analytical, not computational, and not requiring trajectories or sampling. So it is orders of magnitude faster to compute.

Most importantly, the Cage Water model gives a remarkably simple interpretation of water's anomalies, as transitions among the three bond types. Ice melts when small populations of cages convert to small populations of vdW bonds in a large background sea of pairwise Hbonds. Water's supercooling liquid-liquid transition happens when water cages melt into pairwise Hbonds in a small background sea of vdW bonding. The minimum in thermal compressibility occurs when cages convert to vdW bonds. The minimum in the heat capacity results from the conversion of cages to pHB. The crossover from negative to positive thermal expansion in cold water is a transition from pHB to vdW states.

Acknowledgments

We acknowledge the funding from NIH Grant RM1 GM135136 and the Laufer Center for Physical and Quantitative Biology at Stony Brook University. We thank Tomaz Urbic for fruitful discussions and for sharing the code for the CageWater (UD) model.

References

[1] Aneesur Rahman and Frank H Stillinger. Molecular dynamics study of liquid water. *The Journal of Chemical Physics*, 55(7):3442–3449, 1971.

[2] William L. Jorgensen. Transferable Intermolecular Potential Functions for Water, Alcohols, and Ethers. Application to Liquid Water. *Journal of the American Chemical Society*, 103(2):335–340, 1981.

[3] J. L.F. Abascal and C. Vega. A general purpose model for the condensed phases of water: TIP4P/2005. *Journal of Chemical Physics*, 123(23), 2005.

[4] H. J.C. Berendsen, J. R. Grigera, and T. P. Straatsma. The missing term in effective pair potentials. *Journal of Physical Chemistry*, 91(24):6269–6271, 1987.

[5] Valeria Molinero and Emily B. Moore. Water modeled as an intermediate element between carbon and silicon. *Journal of Physical Chemistry B*, 113(13):4008–4016, apr 2009.

[6] Saeed Izadi, Ramu Anandakrishnan, and Alexey V. Onufriev. Building water models: A different approach. *Journal of Physical Chemistry Letters*, 5(21):3863–3871, nov 2014.

[7] Gregory R. Medders, Volodymyr Babin, and Francesco Paesani. Development of a "first-principles" water potential with flexible monomers. iii. liquid phase properties. *Journal of Chemical Theory and Computation*, 10(8):2906–2910, 2014. PMID: 26588266.

[8] Yuriy Khalak, Björn Baumeier, and Mikko Karttunen. Improved general-purpose five-point model for water: TIP5P/2018. *Journal of Chemical Physics*, 149(22):224507, 2018.

[9] Raymond Weldon and Feng Wang. Water Potential from Adaptive Force Matching for Ice and Liquid with Revised Dispersion Predicts Supercooled Liquid Anomalies in Good Agreement with Two Independent Experimental Fits. *Journal of Physical Chemistry B*, 128(14):3398–3407, apr 2024.

[10] Etienne Palos, Ethan F. Bull-Vulpe, Xuanyu Zhu, Henry Agnew, Shreya Gupta, Suman Saha, and Francesco Paesani. Current Status of the MB-pol Data-Driven Many-Body Potential for Predictive Simulations of Water Across Different Phases. *Journal of Chemical Theory and Computation*, 20:21, nov 2024.

[11] Christian J. Burnham and Sotiris S. Xantheas. Development of transferable interaction models for water. III. Reparametrization of an all-atom polarizable rigid model (TTM2–R) from first principles. *The Journal of Chemical Physics*, 116(4):1500–1510, 01 2002.

[12] Lee-Ping Wang, Teresa Head-Gordon, Jay W. Ponder, Pengyu Ren, John D. Chodera, Peter K. Eastman, Todd J. Martinez, and Vijay S. Pande. Systematic improvement of a

classical molecular model of water. *The Journal of Physical Chemistry B*, 117(34):9956–9972, 2013. PMID: 23750713.

[13] Sandeep K. Reddy, Shelby C. Straight, Pushp Bajaj, C. Huy Pham, Marc Riera, Daniel R. Moberg, Miguel A. Morales, Chris Knight, Andreas W. Götz, and Francesco Paesani. On the accuracy of the mb-pol many-body potential for water: Interaction energies, vibrational frequencies, and classical thermodynamic and dynamical properties from clusters to liquid water and ice. *The Journal of Chemical Physics*, 145(19):194504, 11 2016.

[14] Akshaya K. Das, Lars Urban, Itai Leven, Matthias Loipersberger, Abdulrahman Aldossary, Martin Head-Gordon, and Teresa Head-Gordon. Development of an advanced force field for water using variational energy decomposition analysis. *Journal of Chemical Theory and Computation*, 15(9):5001–5013, 2019. PMID: 31408601.

[15] Eleftherios Lambros and Francesco Paesani. How good are polarizable and flexible models for water: Insights from a many-body perspective. *The Journal of Chemical Physics*, 153(6):060901, 08 2020.

[16] Tobias Morawietz, Andreas Singraber, Christoph Dellago, and Jörg Behler. How van der waals interactions determine the unique properties of water. *Proceedings of the National Academy of Sciences of the United States of America*, 113:8368–8373, 7 2016.

[17] Andreas Singraber, Tobias Morawietz, Jörg Behler, and Christoph Dellago. Density anomaly of water at negative pressures from first principles. *Journal of Physics: Condensed Matter*, 30:254005, 6 2018.

[18] Henry Chan, Mathew J. Cherukara, Badri Narayanan, Troy D. Loeffler, Chris Benmore, Stephen K. Gray, and Subramanian K.R.S. Sankaranarayanan. Machine learning coarse grained models for water. *Nature Communications*, 10(1):1–14, 2019.

[19] Aleks Reinhardt and Bingqing Cheng. Quantum-mechanical exploration of the phase diagram of water. *Nature Communications 2021 12:1*, 12:1–7, 1 2021.

[20] Oliver Wohlfahrt, Christoph Dellago, and Marcello Sega. Ab initio structure and thermodynamics of the rpbe-d3 water/vapor interface by neural-network molecular dynamics. *Journal of Chemical Physics*, 153, 10 2020.

[21] Amir Omranpour, Pablo Montero De Hijes, Jörg Behler, and Christoph Dellago. Perspective: Atomistic simulations of water and aqueous systems with machine learning potentials. *Journal of Chemical Physics*, 160, 5 2024.

[22] Pablo Montero de Hijes, Christoph Dellago, Ryosuke Jinnouchi, Bernhard Schmiedmayer, and Georg Kresse. Comparing machine learning potentials for water: Kernel-based regression and behler-parrinello neural networks. *Journal of Chemical Physics*, 160, 3 2024.

[23] Jinfeng Liu, Jinggang Lan, and Xiao He. Toward high-level machine learning potential for water based on quantum fragmentation and neural networks. *The Journal of Physical Chemistry A*, 126(24):3926–3936, 2022. PMID: 35679610.

[24] Sigbjørn Løland Bore and Francesco Paesani. Realistic phase diagram of water from "first principles" data-driven quantum simulations. *Nature Communications 2023 14:1*, 14(1):1–10, jun 2023.

[25] Numa Zorzi, Andreas Neophytou, and Francesco Sciortino. Two state model for the ML-BOP potential. *Molecular Physics*, 2024.

[26] Peter H. Poole, Francesco Sciortino, Ulrich Essmann, and H. Eugene Stanley. Phase behaviour of metastable water. *Nature 1992 360:6402*, 360(6402):324–328, 1992.

[27] David T Limmer and David Chandler. The putative liquid-liquid transition is a liquid-solid transition in atomistic models of water. *Journal of Chemical Physics*, 135(13):134503, 2011.

[28] David T Limmer and David Chandler. The putative liquid-liquid transition is a liquid-solid transition in atomistic models of water. II. *THE JOURNAL OF CHEMICAL PHYSICS*, 138:214504, 2013.

[29] Jeremy C. Palmer, Fausto Martelli, Yang Liu, Roberto Car, Athanassios Z. Panagiotopoulos, and Pablo G. Debenedetti. Metastable liquid–liquid transition in a molecular model of water. *Nature 2014 510:7505*, 510(7505):385–388, jun 2014.

[30] Pablo G. Debenedetti, Francesco Sciortino, and Gül H. Zerze. Second critical point in two realistic models of water. *Science*, 369(6501):289–292, 2020.

[31] W. C. Röntgen. Ueber die Constitution des flüssigen Wassers. *Annalen der Physik*, 281(1):91–97, jan 1892.

[32] J. D. Bernal and R. H. Fowler. A Theory of Water and Ionic Solution, with Particular Reference to Hydrogen and Hydroxyl Ions. *The Journal of Chemical Physics*, 1(8):515–548, 08 1933.

[33] Linus Pauling. The structure and entropy of ice and of other crystals with some randomness of atomic arrangement. *J. Am. Chem. Soc.*, 57:2680–2684, 1935.

[34] John Anthony Pople and John Edward Lennard-Jones. Molecular association in liquids ii. a theory of the structure of water. *Proceedings of the Royal Society of London. Series A. Mathematical and Physical Sciences*, 205(1081):163–178, 1951.

[35] C. M. Davis Jr. and T. A. Litovitz. Two-State Theory of the Structure of Water. *The Journal of Chemical Physics*, 42(7):2563–2576, 04 1965.

[36] C Austen Angell. Two-State Thermodynamics and Transport Properties for Water as Zeroth-Order Results of a "Bond Lattice" Model. *The Journal of Physical Chemistry*, 34(4):42, 1961.

[37] Peter H. Poole, Francesco Sciortino, Tor Grande, H Eugene Stanley, and C. Austen Angell. Effect of hydrogen bonds on the thermodynamic behavior of liquid water. *Physical Review Letters*, 73(12):1632–1635, 1994.

[38] Thomas M. Truskett, Pablo G. Debenedetti, Srikanth Sastry, and Salvatore Torquato. A single-bond approach to orientation-dependent interactions and its implications for liquid water. *Journal of Chemical Physics*, 111(6):2647–2651, aug 1999.

[39] Hajime Tanaka. Simple physical model of liquid water. *Journal of Chemical Physics*, 112(2):799–809, 2000.

[40] C. E. Bertrand and M. A. Anisimov. Peculiar thermodynamics of the second critical point in supercooled water. *Journal of Physical Chemistry B*, 115(48):14099–14111, dec 2011.

[41] V Holten, C E Bertrand, M A Anisimov, and J V Sengers. Thermodynamics of supercooled water. *Journal of Chemical Physics*, 136(9), 2012.

[42] Paola Gallo, Katrin Amann-Winkel, Charles Austen Angell, Mikhail Alexeevich Anisimov, Frédéric Caupin, Charusita Chakravarty, Erik Lascaris, Thomas Loerting, Athanassios Zois Panagiotopoulos, John Russo, Jonas Alexander Sellberg, Harry Eugene Stanley, Hajime Tanaka, Carlos Vega, Limei Xu, and Lars Gunnar Moody Pettersson. Water: A Tale of Two Liquids. *Chemical Reviews*, 116(13):7463–7500, jul 2016.

[43] Tomaz Urbic and Ken A Dill. Water is a cagey liquid. *Journal of the American Chemical Society*, 140(49):17106–17113, 2018.

[44] Giancarlo Franzese, Manuel I. Marqués, and H. Eugene Stanley. Intramolecular coupling as a mechanism for a liquid-liquid phase transition. *Physical Review E - Statistical Physics, Plasmas, Fluids, and Related Interdisciplinary Topics*, 67(1):7, 2003.

[45] Giancarlo Franzese and H Eugene Stanley. The Widom line of supercooled water. *J. Phys.: Condens. Matter*, 19:16, 2007.

[46] Luis Enrique Coronas, Oriol Vilanova, and Giancarlo Franzese. A transferable molecular model for accurate thermodynamic studies of water in large-scale systems. *PREPRINT (Version 1) available at Research Square [https://doi.org/10.21203/rs.3.rs-4243098/v1]*, 16 April 2024.

[47] Tomaz Urbic and Ken A. Dill. A statistical mechanical theory for a two-dimensional model of water. *The Journal of Chemical Physics*, 132(22):224507, jun 2010.

[48] Thomas M. Truskett and Ken A. Dill. A simple statistical mechanical model of water. *Journal of Physical Chemistry B*, 106(45):11829–11842, nov 2002.

[49] Ken A. Dill and Sarina Bromberg. *Molecular Driving Forces. Statistical Thermodynamics in Biology, Chemistry, Physics, and Nanoscience*. Garland Science, Taylor & Francis Group, 2 edition, 2011.

[50] Tomaz Urbic. Analytical model for three-dimensional Mercedes-Benz water molecules. *Physical Review E*, 85:61503, 2012.

[51] Miguel A González, Chantal Valeriani, Frédéric Caupin, and José L.F. Abascal. A comprehensive scenario of the thermodynamic anomalies of water using the TIP4P/2005 model. *Journal of Chemical Physics*, 145(5):54505, 2016.

[52] Osamu Mishima. Volume of supercooled water under pressure and the liquid-liquid critical point. *Journal of Chemical Physics*, 133(14):144503, 2010.

[53] Gaël Pallares, Miguel A. Gonzalez, Jose Luis F. Abascal, Chantal Valeriani, and Frédéric Caupin. Equation of state for water and its line of density maxima down to -120 MPa. *Physical Chemistry Chemical Physics*, 18(8):5896–5900, feb 2016.

[54] F. Sciortino, Y. Zhai, S. L. Bore, and F. Paesani. Constraints on the location of the liquid–liquid critical point in water. *Nature Physics 2025*, 5:1–23, feb 2025.

[55] Frédéric Caupin and Mikhail A. Anisimov. Thermodynamics of supercooled and stretched water: Unifying two-structure description and liquid-vapor spinodal. *Journal of Chemical Physics*, 151(3):34503, jul 2019.

[56] Maria Antonietta Ricci, Fabio Bruni, and Alessia Giuliani. "Similarities" between confined and supercooled water. *Faraday Discussions*, 141(0):347–358, nov 2008.

[57] C. A. Angell, M. Oguni, and W. J. Sichina. Heat capacity of water at extremes of supercooling and superheating. *Journal of Physical Chemistry*, 86(6):998–1002, 1982.

[58] Francesco Mallamace, Carmelo Corsaro, Domenico Mallamace, Sebastiano Vasi, Cirino Vasi, and H Eugene Stanley. Thermodynamic properties of bulk and confined water. *Journal of Chemical Physics*, 141(18):18–504, 2014.

[59] C. W. Lin and J. P.M. Trusler. The speed of sound and derived thermodynamic properties of pure water at temperatures between (253 and 473) K and at pressures up to 400 MPa. *Journal of Chemical Physics*, 136(9):94511, mar 2012.

[60] Harshad Pathak, Alexander Späh, Niloofar Esmaeildoost, Jonas A. Sellberg, Kyung Hwan Kim, Fivos Perakis, Katrin Amann-Winkel, Marjorie Ladd-Parada, Jayanath Koliyadu, Thomas J. Lane, Cheolhee Yang, Henrik Till Lemke, Alexander Roland Oggenfuss, Philip J.M. Johnson, Yunpei Deng, Serhane Zerdane, Roman Mankowsky, Paul Beaud, and Anders Nilsson. Enhancement and maximum in the isobaric specific-heat capacity measurements of deeply supercooled water using ultrafast calorimetry. *Proceedings of the National Academy of Sciences of the United States of America*, 118:e2018379118, 2 2021.

[61] Pablo G Debenedetti. Supercooled and glassy water. *J. Phys.: Condens. Matter*, 15:1669–1726, 2003.

[62] F. Mallamace, C. Corsaro, M. Broccio, C. Branca, N. González-Segredo, J. Spooren, S. H. Chen, and H. E. Stanley. NMR evidence of a sharp change in a measure of local order in deeply supercooled confined water. *Proceedings of the National Academy of Sciences of the United States of America*, 105(35):12725–12729, sep 2008.

[63] M. Oguni, Y. Kanke, and S. Namba. Thermal Properties of the Water Confined within Nanopores of Silica MCM-41. *AIP Conference Proceedings*, 982(1):34–38, 02 2008.

[64] John W. Biddle, Rakesh S. Singh, Evan M. Sparano, Francesco Ricci, Miguel A. González, Chantal Valeriani, José L.F. Abascal, Pablo G. Debenedetti, Mikhail A. Anisimov, and Frédéric Caupin. Two-structure thermodynamics for the TIP4P/2005 model of water covering supercooled and deeply stretched regions. *Journal of Chemical Physics*, 146(3):34502, jan 2017.

[65] Vincent Holten, Jeremy C. Palmer, Peter H. Poole, Pablo G. Debenedetti, and Mikhail A. Anisimov. Two-state thermodynamics of the ST2 model for supercooled water. *The Journal of Chemical Physics*, 140(10):104502, 03 2014.

[66] Chen-Tung Chen, Rana A Fine, and Frank J Millero. The equation of state of pure water determined from sound speeds. *J. Chem. Phys*, 66:2142–2144, 1977.

[67] Kyung Hwan Kim, A. Späh, Harshad Pathak, Fivos Perakis, Daniel Mariedahl, Katrin Amann-Winkel, Jonas A. Sellberg, Jae Hyuk Lee, Sangsoo Kim, Jaehyun Park, Ki Hyun Nam, Tetsuo Katayama, and Anders Nilsson. Maxima in the thermodynamic response and correlation functions of deeply supercooled water. *Science*, 358(6370):1589–1593, dec 2017.

[68] Vincent Holten, Chen Qiu, Emmanuel Guillerm, Max Wilke, Jaroslav Rička, Martin Frenz, and Frédéric Caupin. Compressibility anomalies in stretched water and their interplay with density anomalies. *The Journal of Physical Chemistry Letters*, 8(22):5519–5522, 2017. PMID: 29043801.

[69] Francesco Mallamace, Carmelo Corsaro, and H. Eugene Stanley. Possible relation of water structural relaxation to water anomalies. *Proceedings of the National Academy of Sciences of the United States of America*, 110(13):4899–4904, mar 2013.

[70] José L. F. Abascal and Carlos Vega. Widom line and the liquid–liquid critical point for the TIP4P/2005 water model. *The Journal of Chemical Physics*, 133(23):234502, 12 2010.

[71] Yicun Ni and J. L. Skinner. Evidence for a liquid-liquid critical point in supercooled water within the E3B3 model and a possible interpretation of the kink in the homogeneous nucleation line. *Journal of Chemical Physics*, 144(21):214501, jun 2016.

[72] Robin Tyburski and Anders Nilsson. The structure of water from hot to supercooled temperatures based on analysis of experimental X-ray scattering data. *Molecular Physics*, 2024.

[73] Francesco Mallamace. The liquid water polymorphism. *Proceedings of the National Academy of Sciences of the United States of America*, 106(36):15097–15098, sep 2009.

[74] Peter H Poole, Ivan Saika-Voivod, and Francesco Sciortino. Density minimum and liquid-liquid phase transition. *J. Phys.: Condens. Matter*, 17:431–437, 2005.

[75] Yang Liu, Athanassios Z. Panagiotopoulos, and Pablo G. Debenedetti. Low-temperature fluid-phase behavior of ST2 water. *Journal of Chemical Physics*, 131(10):104508, sep 2009.

[76] Megan J. Cuthbertson and Peter H. Poole. Mixturelike behavior near a liquid-liquid phase transition in simulations of supercooled water. *Phys. Rev. Lett.*, 106:115706, Mar 2011.

[77] Masako Yamada, Stefano Mossa, H. Eugene Stanley, and Francesco Sciortino. Interplay between time-temperature transformation and the liquid-liquid phase transition in water. *Phys. Rev. Lett.*, 88:195701, Apr 2002.

[78] Dietmar Paschek. How the liquid-liquid transition affects hydrophobic hydration in deeply supercooled water. *Physical Review Letters*, 94(21):3–6, 2005.

[79] Dietmar Paschek, Andreas Rüppert, and Alfons Geiger. Thermodynamic and structural characterization of the transformation from a metastable low-density to a very high-density form of supercooled TIP4P-Ew model water. *ChemPhysChem*, 9(18):2737–2741, dec 2008.

[80] D. Corradini, M. Rovere, and P. Gallo. A route to explain water anomalies from results on an aqueous solution of salt. *Journal of Chemical Physics*, 132(13):134508, apr 2010.

[81] Thomas E. Gartner, Pablo M Piaggi, Roberto Car, Athanassios Z Panagiotopoulos, and Pablo G Debenedetti. Liquid-Liquid Transition in Water from First Principles. *Physical Review Letters*, 129(25), 2022.

[82] Jorge R. Espinosa, Jose Luis F. Abascal, Lucia F. Sedano, Eduardo Sanz, and Carlos Vega. On the possible locus of the liquid–liquid critical point in real water from studies of supercooled water using the tip4p/ice model. *The Journal of Chemical Physics*, 158(20):204505, 05 2023.

[83] Debdas Dhabal, Rajat Kumar, and Valeria Molinero. Liquid–liquid transition and ice crystallization in a machine-learned coarse-grained water model. *Proceedings of the National Academy of Sciences of the United States of America*, 121(20):e2322853121, may 2024.

[84] Luis Enrique Coronas and Giancarlo Franzese. Phase behavior of metastable water from large-scale simulations of a quantitative accurate model: The liquid-liquid critical point. *The Journal of Chemical Physics*, 161(16):164502, may 2024.

[85] Osamu Mishima and Tatsuya Sumita. Equation of State of Liquid Water Written by Simple Experimental Polynomials and the Liquid-Liquid Critical Point. *Journal of Physical Chemistry B*, 127(6):1414–1421, feb 2023.

[86] J. A. Sellberg, C. Huang, T. A. McQueen, N. D. Loh, H. Laksmono, D. Schlesinger, R. G. Sierra, D. Nordlund, C. Y. Hampton, D. Starodub, D. P. Deponte, M. Beye, C. Chen, A. V. Martin, A. Barty, K. T. Wikfeldt, T. M. Weiss, C. Caronna, J. Feldkamp, L. B. Skinner, M. M. Seibert, M. Messerschmidt, G. J. Williams, S. Boutet, L. G.M. Pettersson, M. J. Bogan, and A. Nilsson. Ultrafast X-ray probing of water structure below the homogeneous ice nucleation temperature. *Nature 2014 510:7505*, 510(7505):381–384, jun 2014.

[87] Kyung Hwan Kim, Katrin Amann-Winkel, Nicolas Giovambattista, Alexander Späh, Fivos Perakis, Harshad Pathak, Marjorie Ladd Parada, Cheolhee Yang, Daniel Mariedahl, Tobias Eklund, Thomas J. Lane, Seonju You, Sangmin Jeong, Matthew Weston, Jae Hyuk Lee, Intae Eom, Minseok Kim, Jaeku Park, Sae Hwan Chun, Peter H. Poole, and Anders Nilsson. Experimental observation of the liquid-liquid transition in bulk supercooled water under pressure. *Science*, 370(6519):978–982, nov 2020.

[88] Anders Nilsson. Origin of the anomalous properties in supercooled water based on experimental probing inside "no-man's land". *Journal of Non-Crystalline Solids: X*, 14:100095, 2022.

[89] Katrin Amann-Winkel, Kyung Hwan Kim, Nicolas Giovambattista, Marjorie Ladd-Parada, Alexander Späh, Fivos Perakis, Harshad Pathak, Cheolhee Yang, Tobias Eklund, Thomas J. Lane, Seonju You, Sangmin Jeong, Jae Hyuk Lee, Intae Eom, Minseok Kim, Jaeku Park, Sae Hwan Chun, Peter H. Poole, and Anders Nilsson. Liquid-liquid phase separation in supercooled water from ultrafast heating of low-density amorphous ice. *Nature Communications*, 14(1):2–9, 2023.

[90] Gaël Pallares, Mouna El Mekki Azouzi, Miguel A. González, Juan L. Aragones, José L. F. Abascal, Chantal Valeriani, and Frédéric Caupin. Anomalies in bulk supercooled water at negative pressure. *Proceedings of the National Academy of Sciences of the United States of America*, 111(22):7936–7941, jun 2014.

[91] K T Wikfeldt, A Nilsson, and L. G.M. Pettersson. Spatially inhomogeneous bimodal inherent structure of simulated liquid water. *Physical Chemistry Chemical Physics*, 13(44):19918–19924, 2011.

[92] Biswajit Santra, Robert A. DiStasio, Fausto Martelli, and Roberto Car. Local structure analysis in ab initio liquid water. *Molecular Physics*, 113(17-18):2829–2841, sep 2015.

[93] Niall J English and John S Tse. Density fluctuations in liquid water. *Physical Review Letters*, 106(3), 2011.

[94] Frank Smallenburg and Francesco Sciortino. Tuning the Liquid-Liquid Transition by Modulating the Hydrogen-Bond Angular Flexibility in a Model for Water. *Physical Review Letters*, 115(1), 2015.

[95] Tomohiro Sotani, Jacek Arabas, Hironobu Kubota, Masamichi Kijima, and Shoji Asada. Volumetric behaviour of water under high pressure at subzero temperature. *High Temperatures - High Pressures*, 32(4):433–440, 2000.

[96] Douglas R. Caldwell. The maximum density points of pure and saline water. *Deep Sea Research*, 25(2):175–181, 1978.

[97] P. Gallo, D. Corradini, and M. Rovere. Widom line and dynamical crossovers as routes to understand supercritical water. *Nature Communications*, 5:3–8, 2014.

[98] Rakesh S. Singh, John W. Biddle, Pablo G. Debenedetti, and Mikhail A. Anisimov. Two-state thermodynamics and the possibility of a liquid-liquid phase transition in

supercooled TIP4P/2005 water. *Journal of Chemical Physics*, 144(14):144504, apr 2016.

[99] Osamu Mishima and H. Eugene Stanley. Decompression-induced melting of ice IV and the liquid-liquid transition in water. *Nature*, 392(6672):164–166, mar 1998.

[100] Thomas E. Gartner, Kelly M. Hunter, Eleftherios Lambros, Alessandro Caruso, Marc Riera, Gregory R. Medders, Athanassios Z. Panagiotopoulos, Pablo G. Debenedetti, and Francesco Paesani. Anomalies and Local Structure of Liquid Water from Boiling to the Supercooled Regime as Predicted by the Many-Body MB-pol Model. *Journal of Physical Chemistry Letters*, 13(16):3652–3658, apr 2022.

[101] L A Curtiss, ; D J Frurip, ; M Blander, D J Frurip, and M Blander. Absolute infrared intensities of the fundamental absorption bands in solid cyanogen halides. *J. Chem. Phys*, 71:49, 1979.

[102] H. A. Gebbie, W. J. Burroughs, John Chamberlain, J. E. Harries, and R. G. Jones. Dimers of the Water Molecule in the Earth's Atmosphere. *Nature*, 221(5176):143–145, jan 1969.

[103] V. I. Dianov-Klokov, V. M. Ivanov, V. N. Aref'ev, and N. I. Sizov. Water vapour continuum absorption at 8–13 μ. *Journal of Quantitative Spectroscopy and Radiative Transfer*, 25:83–92, 1 1981.

[104] G. V. Bondarenko and Yu E. Gorbaty. An infrared study of water vapour in the temperature range 573–723 k. dimerization enthalpy and absorption intensities for monomer and dimer. *Molecular Physics*, 74:639–647, 10 1991.

[105] Yusuke Jin and Shun ichi Ikawa. Near-infrared spectroscopic study of water at high temperatures and pressures. *J. Chem. Phys*, 119:12432–12438, 2003.

[106] John G Cormier, Joseph T Hodges, and James R Drummond. Infrared water vapor continuum absorption at atmospheric temperatures. *Citation: The Journal of Chemical Physics*, 122:114309, 2005.

[107] T Nakayama, H Fukuda, T Kamikawa, Y Sakamoto, A Sugita, M Kawasaki, T Amano, H Sato, S Sakaki, I Morino, and G Inoue. Effective interaction energy of water dimer at room temperature: An experimental and theoretical study. *J. Chem. Phys*, 127:134302, 2007.

[108] Phyllis A.Y. Fiadzomor, Anthony M. Keen, Robert B. Grant, and Andrew J. Orr-Ewing. Interaction energy of water dimers from pressure broadening of near-ir absorption lines. *Chemical Physics Letters*, 462:188–191, 9 2008.

[109] Blithe E. Rocher-Casterline, Lee C. Chng, Andrew K. Mollner, and Hanna Reisler. Communication: Determination of the bond dissociation energy (d 0) of the water dimer, (h2o)2, by velocity map imaging. *Journal of Chemical Physics*, 134:211101, 6 2011.

[110] Alex Shank, Yimin Wang, Alexey Kaledin, Bastiaan J Braams, and Joel M Bowman. Accurate ab initio and "hybrid" potential energy surfaces, intramolecular vibrational

energies, and classical ir spectrum of the water dimer. *Journal of Chemical Physics*, 130:144314, 2009.

arXiv:2505.02826v1 [cond-mat.stat-mech] 5 May 2025

Supplementary Information: Statistical mechanical theory of liquid water

Lakshmanji Verma *[1] and Ken Dill †[1,2]

[1] *Laufer Center for Physical and Quantitative Biology, Stony Brook University, NY, USA*

[2] *Department of Physics & Department of Chemistry, Stony Brook University, NY, USA*

May 6, 2025

Theory

We model the liquid water cage state in the limit of the Ih ice cage, which consists of 12-membered building units of water cages. We geometrically estimated the equilibrium volume of the cage per water molecule,

$$v_{cage} = \frac{8\sqrt{3}\sigma_{Ih}^3}{9} = A_{cage}\sigma_{Ih}^3, \tag{1}$$

where σ_{Ih} is the water-water distance in the Ih ice cage. To mimic the pressure response of water in cagey liquid, we evaluate the average volume, $\langle v_{cage}\rangle$ at every temperature and pressure. Then we model the liquid HB state and vdW state as a perturbation of the cage water, such that $A_{pHB} = x_{pHB} \times A_{cage}$ and $A_{vdW} = x_{vdW} \times A_{cage}$ where $x_{pHB} = 0.73$ and $x_{vdW} = 1.21$. The volumes of these three states relate as $\langle v_{vdW}\rangle > v_{cage} > v_{pHB}$. For the NI state, we estimate $v_{NI} = v_{vdW} + T/p$.

To capture the expansibility and compressibility of water over the pT range, we assume the volume of each state is Boltzmann distributed and can be estimated as

$$\langle v_j\rangle = \frac{\int_{r_l}^{r_u^j} v_j \exp(-\frac{pv_j}{k_BT})r^2dr}{\int_{r_l}^{r_u^j} \exp(-\frac{pv_j}{k_BT})r^2dr} \tag{2}$$

Here r_l and r_u^j are fractional fluctuation limits in σ_{Ih}. The lower limit $r_l = \sigma_{Ih}(1 - r_d)$ corresponds to the hard core (inaccessible core) of the water molecule, which is the same for

*Contributing author: lakshmanji.verma@stonybrook.edu

†Corresponding author: dill@laufercenter.org

all four states. Whereas the upper limit $r_u^j = \sigma_{Ih}(1+r_j)$, the expansion limit, differs for each state. For NI, we assume that the local volume of each state is $\langle v_{vdW} \rangle$ and it can translate in the limit $0 < r < \infty$ because $r_u^O >> r_l$ which reduces the integral to $\frac{k_B T}{p}$ and average volume per water molecule, $\langle v_{NI} \rangle$, to $\langle v_{vdW} \rangle + \frac{k_B T}{p}$.

The direction HB interaction, equation (3), is modeled with attraction $-\epsilon_{pHB}^0$ that corresponds to minimum energy configuration when HBs are aligned, a restoring orientation-dependent harmonic potential with spring constant κ_θ and reference orientation $\Theta_0 = 0$ or $\cos(\Theta_0) = 1$.

$$\epsilon_{pHB} = -\epsilon_{pHB}^0 + \kappa_\Theta (1 - \cos(\Theta))^2 \; ; \qquad for - \pi/6 <= \Theta <= \pi/6. \tag{3}$$

Interactions in cooperative cages differ from the HB interaction by an additional attractive term, $\epsilon_{cage} = \epsilon_{pHB} - \epsilon_c$. Whereas vdW state only consists of an isotropic attractive term,

$$\epsilon_{vdW} = -\epsilon_{vdW}^0. \tag{4}$$

The interactions would weaken as the water molecules translate relative to each other on compression and expansion due to changes in pT conditions. We estimate this loss of interaction as the penalty by modeling each interaction with a restoring harmonic potential with a spring constant κ_x and equilibrium water-water distance σ_{Ih}. The Boltzmann averaged spring deformation, $\langle \Delta x \rangle$, over the same limit as for volumes is given by,

$$\langle \Delta x \rangle = \frac{\int_{r_l}^{r_u^j} \Delta x \;\; \exp(-\frac{\kappa_x \Delta x^2}{k_B T}) dx}{\int_{r_l}^{r_u^j} \exp(-\frac{\kappa_x \Delta x^2}{k_B T}) dx}. \tag{5}$$

For simplicity, we consider each water in the three states, cage, pHB, and vdW, interacts with four neighboring water molecules. There would be an additional $6k_BT$ to the overall energy per water molecule, which accounts for equally partitioned bond vibration. Therefore, we can estimate the overall energy per water molecule as

$$u_j = -2\epsilon_j + \kappa_x \langle \Delta x \rangle^2 + 6k_B T \tag{6}$$

Overall energy for open or non-interacting (NI) waters is zero i.e. $u_{NI} = 0$.

Now we can write the weight for single water in each state for an isothermal-isobaric (NpT) ensemble with energy u_j and volume v_j per water molecule as

$$\Delta_j = c(T) 4\pi \int_{r_l}^{r_u^j} r^2 dr \exp\left(-\frac{p\langle v_j \rangle}{kT}\right) \int\int\int d\Phi d\Psi d\Theta \exp\left(-\frac{\langle u_j \rangle}{kT}\right) \tag{7}$$

$c(T)$ is the kinetic contributions to the weight which are assumed to be independent of the water state, $4\pi \int r^2 dr$ integrates over the translational degrees of freedom, and $\int\int\int d\Phi d\Psi d\Theta$ integrates over the rotational degrees of freedom.

The weight for the HB state is given by

$$\Delta_{pHB} = c(T)4\pi \int_{r_d}^{r_{pHB}} r^2 \exp\left(-\frac{pv_{pHB}}{k_BT}\right) dr \times 4\pi^2 \ \exp\left(-\frac{-2\epsilon^0_{pHB} - \kappa_x\langle\Delta x\rangle^2_{pHB}}{k_BT}\right) \times \int_{-\pi/6}^{\pi/6} \exp\left(-\frac{2\kappa_\Theta(1-\cos(\Theta))^2}{k_BT}\right) sin(\Theta)d\Theta$$

$$\Delta_{pHB} = c(T)16\pi^3 \ \exp\left(-\frac{-\epsilon^0_{pHB} + \kappa_x\langle\Delta x\rangle^2_{pHB})}{k_BT}\right) \times \frac{-k_BT}{3pA_{pHB}} \exp\left(-\frac{pA_{pHB}r^3}{k_BT}\right)\Bigg|_{r_d}^{r_{pHB}} \times \sqrt{\left(\frac{\pi k_BT}{8\kappa_\Theta}\right)} erf\left[(2-\sqrt{3})\sqrt{\frac{\kappa_\Theta}{2k_BT}}\right] \tag{8}$$

where r_d is the inaccessible volume of water. Δ_{cage} is the same as Δ_{pHB} with an additional term $\exp(-\frac{2\epsilon_c}{k_BT})$ for cooperativity, the limit r_{pHB} replaced with r_{Cage}, and volume coefficient A_{pHB} replaced with A_{cage}. Δ_{vdW} state follows from equation (8) without the rotational term,

$$\Delta_{vdW} = c(T) \times 32\pi^3 \ \exp\left(-\frac{2(-\epsilon^0_{vdW} + \kappa_x\langle\Delta x\rangle^2_{vdW})}{k_BT}\right) \times \frac{-k_BT}{3pA_{vdW}} \exp\left(-\frac{pA_{vdW}r^3}{k_BT}\right)\Bigg|_{r_d}^{r_{vdW}}. \tag{9}$$

In the absence of any interaction and in the translation limit of $0 < r < \infty$, equation (9) further reduces to

$$\Delta_{NI} = c(T) \times \frac{32\pi^3 k_BT}{3pA_{NI}}. \tag{10}$$

For the vapor weight calculation purpose, we have taken $A_{NI} = x_{NI} \times A_{cage}$, where $x_{NI} \approx 1700$, a physically reasonable expansion of water on vaporization.

From these weights for four states of water, we can write the partition function for the 12-membered single cage as

$$Q_1 = (\Delta_{pHB} + \Delta_{vdW} + \Delta_{NI})^{12} - \Delta^{12}_{pHB} + \Delta^{12}_{cage}. \tag{11}$$

Here, the first term accounts for many-body combinations, up to 12th order, of the three water states, pHB, vdW, and NI, contributing to the 12-membered water. We assume that perfectly aligned four hydrogen bonds in the 12-membered cage impart an additional cooperative energy to each water. So, we replace the 12th order pair HB contribution Δ^{12}_{pHB}, 2nd term, from the partition function, Q_1, with Δ^{12}_{cage}, 3rd term to incorporate this cooperative nature of the 12-membered cage. The Partition function for one water effectively would be given by $q_b = Q_1^{1/12}$. Therefore, for a system of N particles, the total partition function would be $Q = q_b^N = Q_1^{(N/3)}$, since each water is part of 4 cages. We then obtain water's thermophysical properties using standard thermodynamic relationships [1] derived in prior works [2, 3, 4, 5].

Attraction energy between cages, beyond pairwise interactions, is modeled with a self-consistent mean-field approach, the same as in the TD model [2], $-a/\langle v_{mol}\rangle$ per water

molecule, where a is the van der Waal type dispersion term between cages and $\langle v_{mol} \rangle$ is the ensembles averaged molar volume of water, at given T and p, given by

$$\langle v_{mol} \rangle = \sum_j f_j \langle v_j \rangle, \tag{12}$$

where f_j is the population of the respective state given by

$$f_j = \frac{\partial \ln Q_1}{\partial \ln \Delta_j^{12}} = \frac{\Delta_j \partial Q_1}{12 Q_1 \partial \Delta_j}. \tag{13}$$

Thermodynamics quantities after turning the mean-field attraction between cages on

It can be shown that turning on the attraction between cages reduces the pressure of the system from p_0 to

$$p = p_0 - a/v_0^2, \tag{14}$$

where p_0 is the pressure exerted by cages without the attraction and p is the effective pressure of the bulk water. Similarly, it can also be shown the the enthalpy reduces from h at pressure p to $h_0 - 2a/v_0$ at pressure p_0 [2].

So, to get the properties at pressure p, we first evaluate them at higher pressure p_0 such that

$$p_0 = p + a/v_0^2. \tag{15}$$

We start from the actual thermodynamic pressure p to self-consistently evaluate p_0 using Eq. 15. Then the water properties at p are calculated using relations from the properties evaluated at p_0. These relations, shown below, can be derived thermodynamically. Note that v_0 is a function of p, p_0, and T.

The relation for the isothermal compressibility, κ_T^p, at p is

$$\kappa_T^p = \frac{\kappa_T^{p_0}}{v_0[1 - \frac{2a}{v_0^2}\kappa_T^{p_0}]}, \tag{16}$$

where $\kappa_T^{p_0}$ is the isothermal compressibility at p_0 such that

$$\begin{aligned} \kappa_T^{p_0} &= -\frac{\partial \ln v_0}{\partial p} = -\frac{1}{v_0}\frac{\partial v_0}{\partial p} = -\frac{1}{v_0} \sum_j \frac{\partial f_j v_{j,0}}{\partial p} \\ &= -\frac{1}{v_0} \sum_j \left[f_j \frac{\partial v_{j,0}}{\partial p} + v_{j,0} \frac{\partial f_j}{\partial p} \right] \equiv \sum_j \kappa_{T,j}^{p_0}. \end{aligned} \tag{17}$$

Here $\kappa_{T,j}^{p_0}$ is the isothermal compressibility of jth state at p_0.

Similarly, the isobaric expansion coefficient, α_p, at p is

$$\alpha_p = \frac{\alpha_{p_0}}{v_0[1 - \frac{2a}{v_0^2}\kappa_T^{p_0}]}, \tag{18}$$

where α_{p_0} is given by

$$\alpha_{p_0} = \frac{\partial \ln v_0}{\partial T} = \frac{1}{v_0} \sum_j \left[f_j \frac{\partial v_{j,0}}{\partial T} + v_{j,0} \frac{\partial f_j}{\partial T} \right] \equiv \sum_j \alpha_{p_0,j}. \tag{19}$$

Here $\alpha_{p_0,j}$ is the expansion coefficient of jth state at p_0.

Finally the heat capacity, C_p at p is given by

$$C_p = \frac{\partial h}{\partial T}\Big|_p = \frac{\partial h}{\partial T}\Big|_{p_0} + \frac{\partial h}{\partial p_0}\Big|_T \frac{\partial p_0}{\partial T}\Big|_p \tag{20}$$

It can also be shown that turning on attraction reduces the enthalpy from h at pressure p to $h_{p_0} - 2a/v_0$ at pressure p_0 [2]. So, it can be shown that Eq. 20 leads to

$$C_p = C_{p_0} + \frac{2a\alpha_{p_0}\kappa_T^{p_0} p_0}{v_0[1 - \frac{2a}{v_0^2}\kappa_T^{p_0}]}. \tag{21}$$

Where C_{p_0} is

$$C_{p_0} = \sum_j \frac{\partial(f_j \langle h_{p_0,j} \rangle)}{\partial T} = \sum_j \left(f_j \frac{\partial \langle h_{p_0,j} \rangle}{\partial T} + \langle h_{p_0,j} \rangle \frac{\partial f_j}{\partial T} \right) \equiv \sum_j C_{p_0,j}, \tag{22}$$

here $h_{p_0,j}$ and $C_{p_0,j}$ are enthalpy and heat capacity of jth state at p_0, respectively.

Model parameters

To find the optimum parameters we used PyGAD [6], a genetic algorithm Python library, to search the multidimensional bound parameter space to minimize the error between predicted and selected experimental data [7, 5, 8, 9, 10, 11, 12]. Table 1 lists the optimized parameters used in this study. All parameters are rounded off to 3 significant digits.

Table 1: Parameters of the current model

Parameters	**Description**	**Values**
r_{Ih}	Equilibrium HB length in Ih ice	2.77 Å
r_{Cage}^{max}	Cooperative HB length maximum	2.97 Å
r_{pHB}^{max}	Pair HB length maximum	3.23 Å
r_{vdW}^{max}	van der Waals bond length maximum	3.53 Å
r_d	Inaccessible hardcore size of water	2.63 Å
x_{pHB}	pHB water volume perturbation factor	0.724
x_{vdW}	vdW water volume perturbation factor	1.29
x_{NI}	Water vapor volume perturbation factor	1700
ϵ_{Cage}^0	Cooperative HB maximum interaction potential	20.5 kJmol^{-1}
ϵ_{pHB}^0	Pair HB maximum interaction potential	19.2 kJmol^{-1}
ϵ_{vdW}^0	Pair vdW maximum interaction potential	10.3 kJmol^{-1}
κ_x	Translational spring constant	13.1 kJmol^{-1} Å^{-2}
κ_θ	Rotational spring constant	897 kJmol^{-1}
a	Dispersion interaction constant between cages	274 kJÅ^{3}mol$^-$1

All the water-water bond length parameters (2.63 Å- 3.53 Å) and hydrogen bond parameters are within the experimental range. This model has 14 adjustable parameters which are similar in number to the total of 12 parameters (see Table 2) of the four-point models like TIP4P/05 and OPC.

Table 2: Parameters of the fixed charge atomistic models TIP4P/05 and OPC

Parameters	**Description**	**TIP4P/05**[13]	**OPC**[14]
ϵ_O	LJ dispersion energy of O	0.63627 kJ/mol	0.89036 kJ/mol
ϵ_H	LJ dispersion energy of H	0.0 kJ/mol	0.0 kJ/mol
ϵ_M	LJ dispersion energy of M	0.0 kJ/mol	0.0 kJ/mol
σ_O	LJ size of O	3.1589 Å	3.16655 Å
σ_H	LJ size of H	0.0 Å	0.0 Å
σ_M	LJ size of M	0.0 Å	0.0 Å
q_O	Charge on O	0.0 e	0.0 e
q_M	Charge on M	-1.1128 e	-1.3582 e
q_H	Charge on H	0.5564 e	0.6791 e
r_OH	OH distance	0.9572 Å	0.8724 Å
r_{OM}	OM distance	0.1546 Å	0.1594 Å
$\angle HOH$	HOH angle	104.52°	103.6°

Phase transition and critical point in the supercooled water

Recent experiments indicate the existence of liquid-liquid phase transition (LLPT) [15, 16]; however, huge fluctuation in pressure (from ambient to 350 MPa) makes the location of the liquid-liquid critical point still elusive (LLCP). Figure 7 (in the main article) shows that the current model predicts the LLCP at 176 MPa and 159 K, where extrema in $C_p^{max}, \kappa_T^{max}$, and α_p^{min} collapse on the WL. It also shows the corresponding LLPT and the binodal line. This predicted LLCP is within the range of previously estimated or predicted LLCP using molecular simulations and thermodynamic analyses [17, 18, 19, 20, 21, 22, 23, 24, 25, 26, 27, 28, 29, 30, 31, 32, 33, 34, 35, 36]. The range of predicted critical pressure, $P_c \approx (60 - 360)$ MPa, and critical temperature, $T_c \approx (172 - 250)$ K, is vast. Mishima and Sumita [36] recently predicted $P_c \approx 105 \pm 9$ MPa by extrapolating empirically fitted n^{th} order polynomials ($n = 3..10$) to calculate the pressure from volume and temperature data, $p_{cal} = \sum_{i=0}^{n} c_i V^i T^i$. However, their prediction is contingent upon the order of polynomials and experimental data used for fitting. Additionally, the possibility of over-fitting can't be overruled with 64 adjustable parameters (for the representative 7×7 polynomial). Whereas recent analyses of atomistic simulation data [37, 38, 34] that predict P_c in the vicinity of ≈ 100 MPa, compare κ_T^{max} prediction with experimental value at ambient pressure. They assume that the predicted κ_T^{max} value would be the same as the experimental κ_T^{max} at the same pressure distance from their respective critical points. Often, these models perform poorly at capturing water's volumetric and thermodynamic properties beyond ambient pressure. For example, a sharper κ_T^{max} peak leads to a lower critical pressure compared to a broader peak [37, 38, 39]. Predictions based on analyses ignorant of such effects of water's properties on the location of LLCP could be misleading.

Recent *ab initio* derived water model, rWAIL [30], and DNN surrogate of MB-pol (DNN@MB-pol [31]) place the P_c in the vicinity of 100 MPa. It's worth pointing out here that these models are optimized to predict highly tetrahedral ice polymorph structures [30, 31], in addition to liquid water configurations. Hestand and Skinner [34] noted that several parameters, including but not limited to charges [40], bond flexibility [41] and tetrahedrality [42], and nuclear quantum effect [43], could influence the location of LLCP of water and similar tetrahedral liquid. In particular, Angell and Kapko [42] showed that stronger tetrahedrality leads to a lower critical pressure, which could explain a significantly lower prediction of P_c by models calibrated to reproduce ice structures. This suggests that the predictions of LLCP by water models could be inherently biased due to the choice of experimental properties prioritized in the validation and training schemes.

In comparison, the current model is purely validated against the macroscopic liquid water's experimental data. It predicts water's response function in excellent quantitative agreement with experiments across temperature and pressure (see figures 2 - 5 of the main article). Liquid water is much more dynamic and significantly less tetrahedrally ordered than different ice polymorphs. This could explain the higher critical pressure ($P_c = 176$ MPa) prediction by the current model compared to DNN@MB-pol and rWAIL. Also, extremely slow speed and small system size of such *ab initio* based models make the validation of other response

functions (C_p, κ_T, and α_p) beyond the ambient pressure against experiments extremely difficult. Whereas, the extremely fast nature of our model makes it advantageous over these extremely slow and computationally expensive atomistic models (for comparison GPU accelerated DNN@MB-pol [31] took several months to produce each data point on a system of only 256 water molecules) to quickly recalibrate and help pinpoint the location of LLCP as more experimental data become available in the erstwhile *no man's land* in the near future.

Supporting Figures

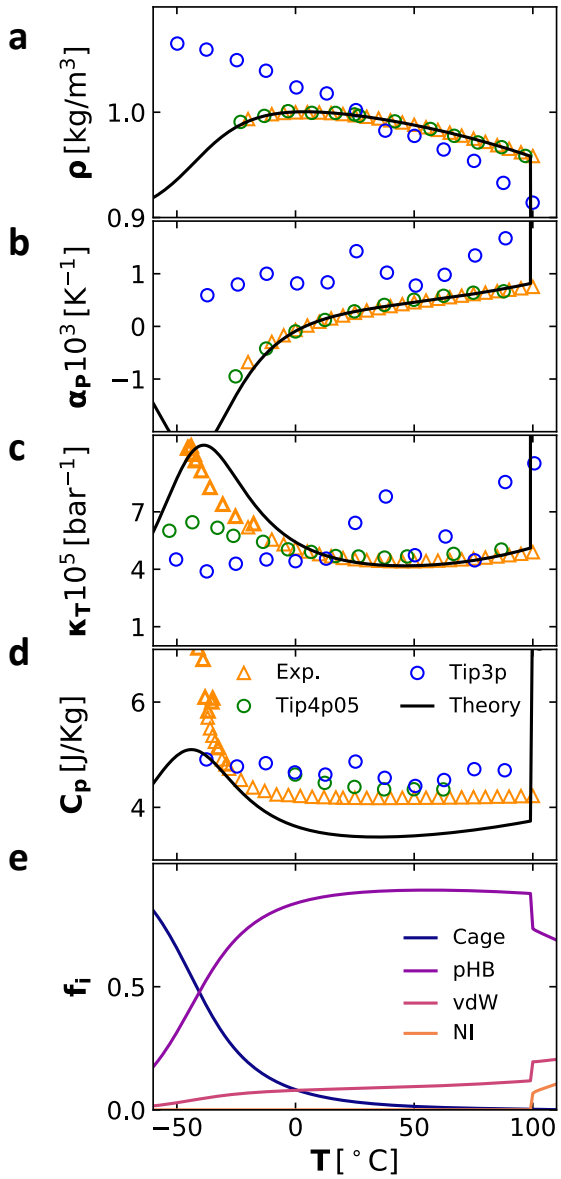

Figure S1: **Comparison with experiments and explicit water model predictions.** Thermophysical properties and population showing first order liquid-vapor transition at 1 atm and 100°C. Theory predictions are shown with lines, experiments with open orange triangles, TIP3P with open blue circles, and TIP4P05 with open green circles. Current predictions are much better than TIP3P water, which is still commonly used in biophysical simulations.

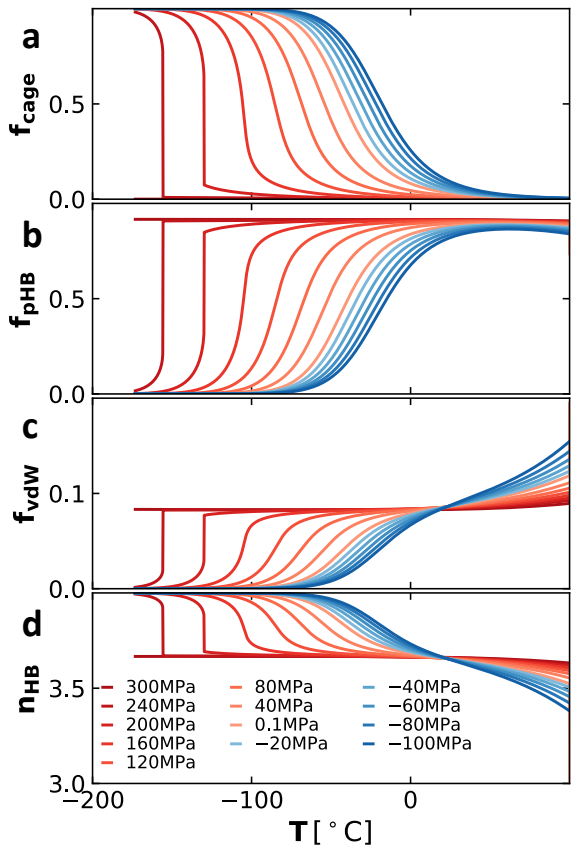

Figure S2: **Isobars of microstates' populations and average hydrogen bond versus temperature.** **a)** cage state. **b)** pHB state. **c)** vdW state. **d)** average hydrogen bonds. $p > 0$ isobars are in shades of red. $p < 0$ isobars are in shades of blue. The Isobar of three states at constant pressure are shown with the same color in both **a)** and **b)**.

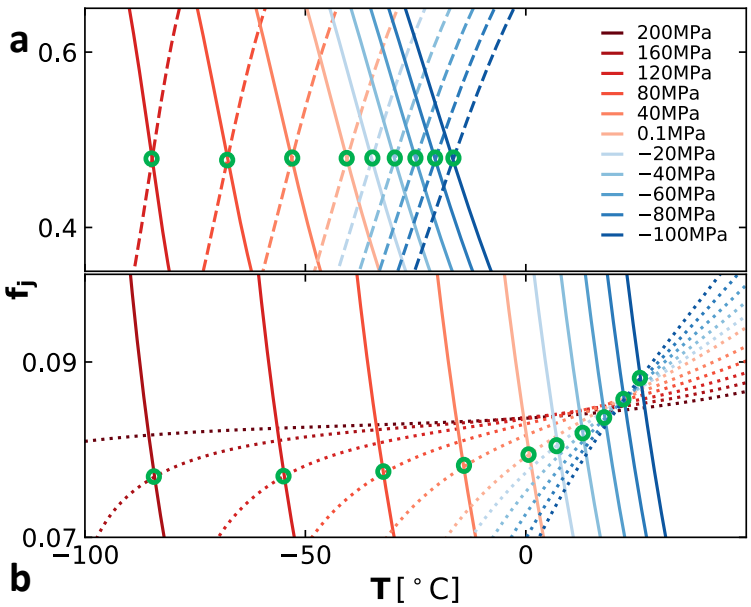

Figure S3: **Crossovers between microstates. a)** Crossovers between f_{cage} (solid lines) and f_{pHB} (dashed lines). **b)** crossovers between f_{cage} (solid lines) and f_{vdW} (dotted line). The crossover points are shown with green open circles.

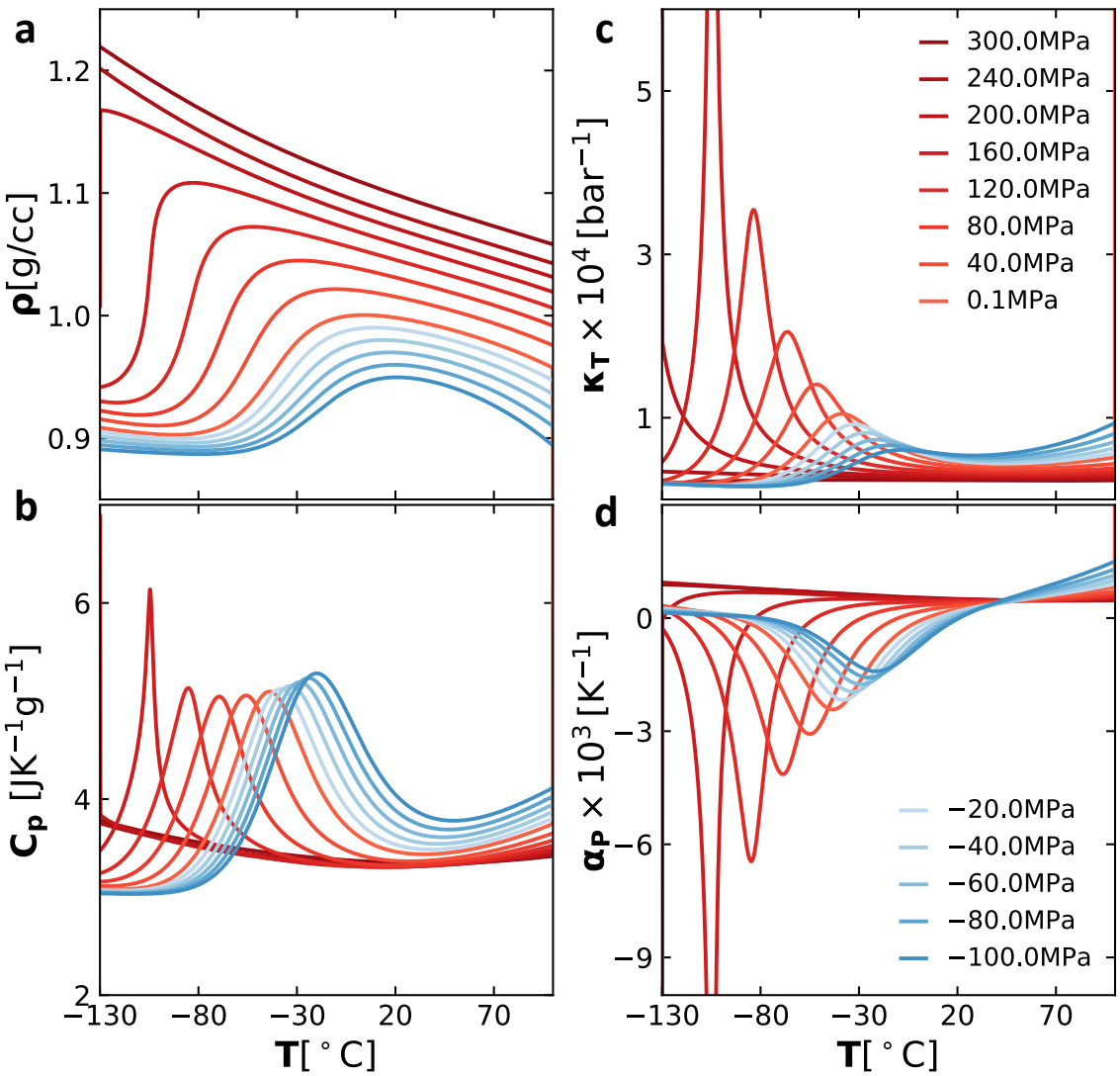

Figure S4: **Isobars predictions of volumetric and energetic responses. a)** Density, ρ, **b)** Heat capacity,C_p. **c)** Isothermal compressibility, κ_T, and **d)** Expansion coefficient, α_p. $p > 0$ isobars are in shades of red. $p < 0$ isobars are in shades of blue. The maximum density, ρ^{max}, and peaks in response functions C_p^{max}, κ_T^{max}, and α_p^{min} shift to a lower temperature with pressure in the supercooled region.

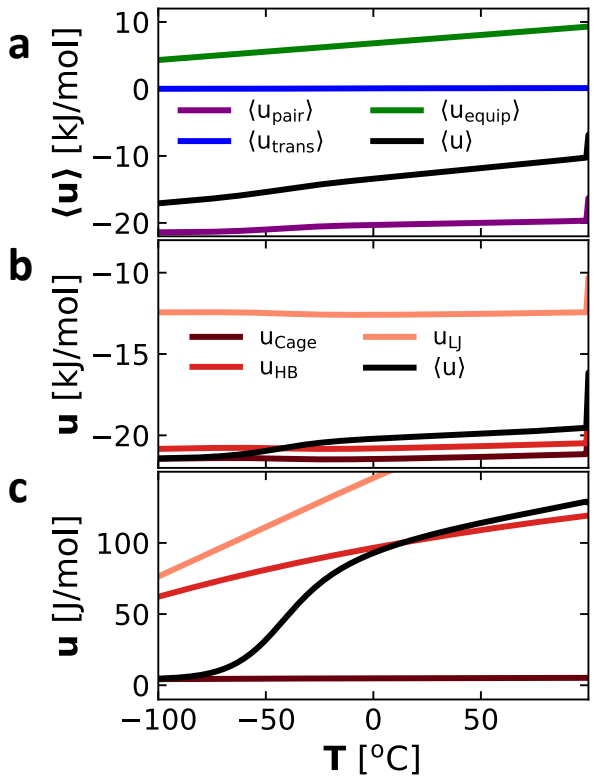

Figure S5: **Average temperature dependent energy contributions per water-water bond.** **a)** Ensemble averaged contributions from pair interaction $\langle\epsilon\rangle$ in purple, translation $\langle u_{trans}\rangle$ in blue, equipartition $\langle u_{equip}\rangle$ in green, and total $\langle u\rangle$ in black. **(b, c)** Energy contribution from different water states; ensemble average $\langle u\rangle$ is in black and state contributions are shown with shades of red. **b)** Without thermal contribution, $6k_BT$ equipartition to bonds. **c)** Transnational contributions.

References

[1] Ken A. Dill and Sarina Bromberg. *Molecular Driving Forces. Statistical Thermodynamics in Biology, Chemistry, Physics, and Nanoscience*. Garland Science, Taylor & Francis Group, 2 edition, 2011.

[2] Thomas M. Truskett and Ken A. Dill. A simple statistical mechanical model of water. *Journal of Physical Chemistry B*, 106(45):11829–11842, nov 2002.

[3] Tomaz Urbic and Ken A. Dill. A statistical mechanical theory for a two-dimensional model of water. *The Journal of Chemical Physics*, 132(22):224507, jun 2010.

[4] Tomaz Urbic. Analytical model for three-dimensional Mercedes-Benz water molecules. *Physical Review E*, 85:61503, 2012.

[5] Tomaz Urbic and Ken A Dill. Water is a cagey liquid. *Journal of the American Chemical Society*, 140(49):17106–17113, 2018.

[6] Ahmed Fawzy Gad. Pygad: An intuitive genetic algorithm python library. *Multim. Tools Appl.*, 83:58029–58042, 2021.

[7] Osamu Mishima. Volume of supercooled water under pressure and the liquid-liquid critical point. *Journal of Chemical Physics*, 133(14):144503, 2010.

[8] Francesco Mallamace, Carmelo Corsaro, Domenico Mallamace, Sebastiano Vasi, Cirino Vasi, and H Eugene Stanley. Thermodynamic properties of bulk and confined water. *Journal of Chemical Physics*, 141(18):18–504, 2014.

[9] C. A. Angell, M. Oguni, and W. J. Sichina. Heat capacity of water at extremes of supercooling and superheating. *Journal of Physical Chemistry*, 86(6):998–1002, 1982.

[10] Chen-Tung Chen, Rana A Fine, and Frank J Millero. The equation of state of pure water determined from sound speeds. *J. Chem. Phys*, 66:2142–2144, 1977.

[11] C. W. Lin and J. P.M. Trusler. The speed of sound and derived thermodynamic properties of pure water at temperatures between (253 and 473) K and at pressures up to 400 MPa. *Journal of Chemical Physics*, 136(9):94511, mar 2012.

[12] Gaël Pallares, Miguel A. Gonzalez, Jose Luis F. Abascal, Chantal Valeriani, and Frédéric Caupin. Equation of state for water and its line of density maxima down to -120 MPa. *Physical Chemistry Chemical Physics*, 18(8):5896–5900, feb 2016.

[13] J. L.F. Abascal and C. Vega. A general purpose model for the condensed phases of water: TIP4P/2005. *Journal of Chemical Physics*, 123(23), 2005.

[14] Saeed Izadi, Ramu Anandakrishnan, and Alexey V. Onufriev. Building water models: A different approach. *Journal of Physical Chemistry Letters*, 5(21):3863–3871, nov 2014.

[15] Kyung Hwan Kim, Katrin Amann-Winkel, Nicolas Giovambattista, Alexander Späh, Fivos Perakis, Harshad Pathak, Marjorie Ladd Parada, Cheolhee Yang, Daniel Mariedahl, Tobias Eklund, Thomas J. Lane, Seonju You, Sangmin Jeong, Matthew Weston, Jae Hyuk Lee, Intae Eom, Minseok Kim, Jaeku Park, Sae Hwan Chun, Peter H.

Poole, and Anders Nilsson. Experimental observation of the liquid-liquid transition in bulk supercooled water under pressure. *Science*, 370(6519):978–982, nov 2020.

[16] Harshad Pathak, Alexander Späh, Niloofar Esmaeildoost, Jonas A. Sellberg, Kyung Hwan Kim, Fivos Perakis, Katrin Amann-Winkel, Marjorie Ladd-Parada, Jayanath Koliyadu, Thomas J. Lane, Cheolhee Yang, Henrik Till Lemke, Alexander Roland Oggenfuss, Philip J.M. Johnson, Yunpei Deng, Serhane Zerdane, Roman Mankowsky, Paul Beaud, and Anders Nilsson. Enhancement and maximum in the isobaric specific-heat capacity measurements of deeply supercooled water using ultrafast calorimetry. *Proceedings of the National Academy of Sciences of the United States of America*, 118:e2018379118, 2 2021.

[17] Peter H. Poole, Francesco Sciortino, Ulrich Essmann, and H. Eugene Stanley. Phase behaviour of metastable water. *Nature 1992 360:6402*, 360(6402):324–328, 1992.

[18] Osamu Mishima and H. Eugene Stanley. Decompression-induced melting of ice IV and the liquid-liquid transition in water. *Nature*, 392(6672):164–166, mar 1998.

[19] Peter H Poole, Ivan Saika-Voivod, and Francesco Sciortino. Density minimum and liquid-liquid phase transition. *J. Phys.: Condens. Matter*, 17:431–437, 2005.

[20] Yang Liu, Athanassios Z. Panagiotopoulos, and Pablo G. Debenedetti. Low-temperature fluid-phase behavior of ST2 water. *Journal of Chemical Physics*, 131(10):104508, sep 2009.

[21] Megan J. Cuthbertson and Peter H. Poole. Mixturelike behavior near a liquid-liquid phase transition in simulations of supercooled water. *Phys. Rev. Lett.*, 106:115706, Mar 2011.

[22] Masako Yamada, Stefano Mossa, H. Eugene Stanley, and Francesco Sciortino. Interplay between time-temperature transformation and the liquid-liquid phase transition in water. *Phys. Rev. Lett.*, 88:195701, Apr 2002.

[23] Dietmar Paschek. How the liquid-liquid transition affects hydrophobic hydration in deeply supercooled water. *Physical Review Letters*, 94(21):3–6, 2005.

[24] Dietmar Paschek, Andreas Rüppert, and Alfons Geiger. Thermodynamic and structural characterization of the transformation from a metastable low-density to a very high-density form of supercooled TIP4P-Ew model water. *ChemPhysChem*, 9(18):2737–2741, dec 2008.

[25] José L. F. Abascal and Carlos Vega. Widom line and the liquid–liquid critical point for the TIP4P/2005 water model. *The Journal of Chemical Physics*, 133(23):234502, 12 2010.

[26] D. Corradini, M. Rovere, and P. Gallo. A route to explain water anomalies from results on an aqueous solution of salt. *Journal of Chemical Physics*, 132(13):134508, apr 2010.

[27] Jeremy C. Palmer, Fausto Martelli, Yang Liu, Roberto Car, Athanassios Z. Panagiotopoulos, and Pablo G. Debenedetti. Metastable liquid–liquid transition in a molecular model of water. *Nature 2014 510:7505*, 510(7505):385–388, jun 2014.

[28] Pablo G. Debenedetti, Francesco Sciortino, and Gül H. Zerze. Second critical point in two realistic models of water. *Science*, 369(6501):289–292, 2020.

[29] Thomas E. Gartner, Pablo M Piaggi, Roberto Car, Athanassios Z Panagiotopoulos, and Pablo G Debenedetti. Liquid-Liquid Transition in Water from First Principles. *Physical Review Letters*, 129(25), 2022.

[30] Raymond Weldon and Feng Wang. Water Potential from Adaptive Force Matching for Ice and Liquid with Revised Dispersion Predicts Supercooled Liquid Anomalies in Good Agreement with Two Independent Experimental Fits. *Journal of Physical Chemistry B*, 128(14):3398–3407, apr 2024.

[31] F. Sciortino, Y. Zhai, S. L. Bore, and F. Paesani. Constraints on the location of the liquid–liquid critical point in water. *Nature Physics 2025*, 5:1–23, feb 2025.

[32] Debdas Dhabal, Rajat Kumar, and Valeria Molinero. Liquid–liquid transition and ice crystallization in a machine-learned coarse-grained water model. *Proceedings of the National Academy of Sciences of the United States of America*, 121(20):e2322853121, may 2024.

[33] Luis Enrique Coronas and Giancarlo Franzese. Phase behavior of metastable water from large-scale simulations of a quantitative accurate model: The liquid-liquid critical point. *The Journal of Chemical Physics*, 161(16):164502, may 2024.

[34] Nicholas J. Hestand and J. L. Skinner. Perspective: Crossing the Widom line in no man's land: Experiments, simulations, and the location of the liquid-liquid critical point in supercooled water. *Journal of Chemical Physics*, 149(14):140901, oct 2018.

[35] Yicun Ni and J. L. Skinner. Evidence for a liquid-liquid critical point in supercooled water within the E3B3 model and a possible interpretation of the kink in the homogeneous nucleation line. *Journal of Chemical Physics*, 144(21):214501, jun 2016.

[36] Osamu Mishima and Tatsuya Sumita. Equation of State of Liquid Water Written by Simple Experimental Polynomials and the Liquid-Liquid Critical Point. *Journal of Physical Chemistry B*, 127(6):1414–1421, feb 2023.

[37] Kyung Hwan Kim, A. Späh, Harshad Pathak, Fivos Perakis, Daniel Mariedahl, Katrin Amann-Winkel, Jonas A. Sellberg, Jae Hyuk Lee, Sangsoo Kim, Jaehyun Park, Ki Hyun Nam, Tetsuo Katayama, and Anders Nilsson. Maxima in the thermodynamic response and correlation functions of deeply supercooled water. *Science*, 358(6370):1589–1593, dec 2017.

[38] Alexander Späh, Harshad Pathak, Kyung Hwan Kim, Fivos Perakis, Daniel Mariedahl, Katrin Amann-Winkel, Jonas A. Sellberg, Jae Hyuk Lee, Sangsoo Kim, Jaehyun Park, Ki Hyun Nam, Tetsuo Katayama, and Anders Nilsson. Apparent power-law behavior of water's isothermal compressibility and correlation length upon supercooling. *Physical Chemistry Chemical Physics*, 21(1):26–31, dec 2019.

[39] Frédéric Caupin and Mikhail A. Anisimov. Thermodynamics of supercooled and stretched water: Unifying two-structure description and liquid-vapor spinodal. *Journal of Chemical Physics*, 151(3):34503, jul 2019.

[40] Erik Lascaris. Tunable liquid-liquid critical point in an ionic model of silica. *Phys. Rev. Lett.*, 116:125701, Mar 2016.

[41] Frank Smallenburg and Francesco Sciortino. Tuning the Liquid-Liquid Transition by Modulating the Hydrogen-Bond Angular Flexibility in a Model for Water. *Physical Review Letters*, 115(1), 2015.

[42] C. Austen Angell and Vitaliy Kapko. Potential tuning in the S W system. (i) Bringing Tc,2 to ambient pressure, and (II) colliding Tc,2 with the liquid vapor spinodal. *Journal of Statistical Mechanics: Theory and Experiment*, 2016(9), 2016.

[43] Binh Nguyen, Gustavo E. Lopez, and Nicolas Giovambattista. Nuclear quantum effects on the liquid-liquid phase transition of a water-like monatomic liquid. *Physical Chemistry Chemical Physics*, 20(12):8210–8217, mar 2018.